Saudi Pharmaceutical Journal 26 (2018) 546–567

Contents lists available at ScienceDirect

Saudi Pharmaceutical Journal

journal homepage: www.sciencedirect.com

Original article

Inverse docking based screening and identification of protein targets for Cassiarin alkaloids against *Plasmodium falciparum*

Arvind Negi [a,1,*], Nitisha Bhandari [b,1], Bharti Rajesh Kumar Shyamlal [c], Sandeep Chaudhary [c,*]

[a] School of Chemistry, National University of Ireland, University Road, Galway H91 TK33, Ireland
[b] School of Biotechnology, Graphic Era University, Dehradun, Bell Road, Society Area, Clement Town, Dehradun, Uttarakhand 248002, India
[c] Laboratory of Organic and Medicinal Chemistry, Department of Chemistry, National Institute of Technology Jaipur, Jawaharlal Nehru Marg, Jaipur 302017, India

ARTICLE INFO

Article history:
Received 6 December 2017
Accepted 31 January 2018
Available online 2 February 2018

Keywords:
Plasmodium falciparum
Inverse docking
Cassiarin alkaloids
Proteomics

ABSTRACT

Various reports have shown Cassiarin alkaloids, selective *in vitro* activities against various strains of *Plasmodium falciparum* with low cytotoxicity, which indicates their possible candidature as antimalarial drug. However, poor recognition of their protein targets and molecular binding behaviour, certainly limits their exploration as antimalarial drug candidature. To address this, we utilises inverse screening, based on three different docking methodologies in order to find their most putative protein targets. In our study, we screened 1047 protein structures from protein data bank, which belongs to 147 different proteins. Our investigation identified 16 protein targets for Cassiarins. In few cases of identified protein targets, the binding site was poorly studied, which encouraged us to perform comparative sequence and structural studies with their homologous proteins, like as in case of Kelch motif associated protein, Armadillo repeats only protein and Methionine aminopeptidase 1b. In our study, we also found Tryptophanyl-tRNA synthetase and 1-Deoxy-D-Xylose-5-phosphate reductoisomerase proteins are the most common targets for Cassiarins.

© 2018 The Authors. Production and hosting by Elsevier B.V. on behalf of King Saud University. This is an open access article under the CC BY-NC-ND license (http://creativecommons.org/licenses/by-nc-nd/4.0/).

1. Introduction

Malaria is a mosquito-borne infectious disease affecting humans and other animals caused by the protozoan parasite, *Plasmodium*. According to WHO 2015 statistics, 212 million clinical episodes and 429,000 deaths were reported worldwide (Bhatt et al. (2015); World_Health_Organization, 2015; Kamholz, 2016; World_Health_Organization, 2016) and nearly 3.2 billion people are at the risk of malaria, especially children under age of 5 years, pregnant women, immune compromised patients, as well as non-immune migrants (Schumacher and Spinelli, 2012; Negi, 2013; Wells et al., 2015). These large numbers are mainly subjected by *Plasmodium falciparum* (*P. falciparum*), followed by *P. vivax*, *P. ovale*, *P. malariae*, and to some extent *P. knowlesi*. Although in recent years, some profound development has been seen in antimalarial drug discovery, but higher number of resistance cases, mild to moderate selectivity/toxicity ratio of most of the antimalarial drugs, show a need of new scaffolds or new chemical entity (NCE) (Bushell et al., 2017). Moreover, the alkaloid natural product class has been found promising and useful in numerous disease states, as mentioned in these reports (Kayser et al., 2003; Frederich et al., 2008; Özçelik et al., 2011; Singla et al., 2013; Singla et al., 2014). Additionally, alkaloids, such as Quinine, Cryptolepine, Thiaplakortones A–D and their semi or synthetic derivatives (Caniato and Puricelli, 2003; Oliveira et al., 2009) are well studied as antimalarial agents (Cimanga et al., 1997; Davis et al., 2013), showing alkaloidal scaffold inheritance of antiplasmodial activity.

In recent years, various medicinal active natural compounds were reported from a plant, *Cassia siamea* (Leguminosae). Most of these natural compounds are either isolated from leaves (Cassiarin-A, B, G, H, J, K, 5-acetonyl-7-hydroxy-2-methylchromene, Chrobisiamone A) (Morita et al., 2007; Oshimi et al., 2008; Deguchi et al., 2012), or flower (Cassiarin C, D, E, F; 10,11-dihydroanhydrobarakol, anhydrobarakol Cassibiphenol A and Cassibiphenol B) (Thongsaard et al., 2001) (Deguchi et al., 2014),

* Corresponding authors.
E-mail addresses: arvindnegi2301@gmail.com (A. Negi), schaudhary.chy@mnit.ac.in (S. Chaudhary).
[1] Both authors have equal contribution.

Peer review under responsibility of King Saud University.

Production and hosting by Elsevier

https://doi.org/10.1016/j.jsps.2018.01.017
1319-0164/© 2018 The Authors. Production and hosting by Elsevier B.V. on behalf of King Saud University.
This is an open access article under the CC BY-NC-ND license (http://creativecommons.org/licenses/by-nc-nd/4.0/).

or also from twigs (Siamalkaloids A, B, C) (Wu et al., 2016), structures shown in Fig. 1. Surprisingly, Cassiarin-A and Cassiarin-B were found highly selective than Chloroquine against chloroquine sensitive *P. falciparum* 3D7 strain over human breast cancer cell lines (MCF7), as selectivity/cytotoxicity ratio are fairly high, ≥4348, ≥1112, 3281 for Cassiarin-A, B and Chloroquine, respectively (Morita et al., 2009). Furthermore, their antimalarial role was purposed though their vasorelaxation activity, as prompted by nitric oxide production from the endothelium, which might inhibit the host cell surface attachment of the parasite (Morita et al., 2009). In 2009, Oshimi et al. isolated Cassiarins C-E and 10,11-dihydroanhydrobarakol which showed reasonable *in vitro* selectivity against *P. falciparum* 3D7 over human leukaemia cells (HL-60 cell lines) (Oshimi et al., 2009).

1.1. Chemistry

Isoquinoline is the basic alkaloidal core of Cassiarins, which fused with 2-methyl-2*H*-pyran ring at position [4, 8a], forms tricyclic ring and as prototype represented in the structure Cassiarin-C (shown in Fig. 1). Further derivatization at C_2 position of Cassiarin-C, forms Cassiarin D, E and F. The methyl at C_2 in the pyran ring of these isoforms (Cassiarin-C, D and E), can adopt 2 conformations as *R* or *S*. Every isoform has its own structure signature at C_2 position, when compare to Cassiarin-C structure, which has simply a methyl group: (a) Cassiarin-D has $-CH_2-$ tethered 5-propenone-7-hydroxy-4*H*-chromen-4-one functionality at C_2 with regards to Cassiarin-C, as shown in Fig. 1; (c) Cassiarin E is *Bis*-isomer of Cassiarin-C; (d) Cassiarin-F has fused with a toluene ring, to form a tetracyclic ring at position [2,3] of Cassiarin-C and also has further substructure extension in a form of 2-resorcinol propanone functionality, shown in Fig. 1.

In order, to characterize the molecular targets for these Cassiarin alkaloids, we used inverse docking, which is grown as a valuable tool in drug target identification in recent years. Also, helpful in rediscovering the molecular mechanism of polypharmacological active compounds, especially, the natural products and detecting, the possible adverse side targets of existing drugs as in toxicological studies. Previous reports on inverse docking shows implementation of various methodologies, to improve the accuracy and prioritizing the identified targets. Kumar et al. tried to address the limitations of docking scoring schemes with respect to attain confidence in theoretical binding affinities (Kumar et al., 2014). They presented a reverse approach, where they used the pharmacophore features of the ligand as interactions of complementary amino acids of protein cavities (also, called them as "pseudorece ptor"). These pseudoreceptors were then matched with the cavities/ binding sites of the selected protein dataset. They applied this approach on 3 co-crystallized ligands over 28 proteins of Zea mays and provide an application of the total probability and docking energy, in order to acquire confidence in prioritizing the probable protein targets (Kumar et al., 2014). Also, Carvalho et al. adopted a reverse screening strategy based on ligand similarity and target structure, which resulted into, a number of putative protein target candidates for quercetin polypharmacological effects and also successfully correlated them, with previously tested proteins, mainly protein kinases and poly [ADP-ribose] polymerases (Carvalho et al., 2017). In another report, Kumar et al. compared the rank list results from inverse docking and ligand-based similarity search, assist them to prioritize the chitinase as most probable target for kinetin molecule, further supported by experimental data (Kumar et al., 2015). While, few compiled literature reviews on inverse screening and its application are available, related to the drug repositioning (Kharkar et al., 2014) and available target databases/servers (Lee et al., 2016).

However, the selectivity/cytotoxicity profile of these reported Cassiarin alkaloids has been promising in *P. falciparum* but as their protein targets are poorly recognised, which certainly limits their further exploration as antimalarial candidature. To identify their protein targets and acquire significant confidence in prioritising the identified target, we used reverse screening on all available protein targets from protein data bank, using three different placement docking methods.

2. Materials & methods

2.1. Proteins set

All the protein targets for *P. falciparum* were searched on protein data bank, claiming 1047 structures. After filtering off the NMR and low resolved cryo-electron structures from X-ray structures, proteins were selected and arranged in the order of their crystal structure resolution as an individual target, see in Table 2. In most cases, preferences were given to co-crystallised ligand containing protein structures, otherwise the structures without co-crystallised ligand protein were also selected. Later, the self-docking on co-crystallise ligand containing protein targets, was performed to calculate the minimum RMSD values (min. RMSD values) in order, to evaluate the competency of a particular protein in accommodating of its own co-crystallise ligand (also, called ligandability) (Kumar, 2018). In those structures, which lack co-crystallise ligand, active site finder tool of MOE (Del Carpio et al., 1993; Negi et al., 2013a) was used to find the active surface patches which were saved as dummy atoms for performing the later docking. Also, in certain cases we aligned the target protein sequences with their homologous proteins of other species. These studies involved superposition of three-dimensional structure of the proteins of interest, as to see the overlapped domains and regions with comparative homologous proteins, which could be inferred into key active site residues in those proteins which were poorly studied in the past.

2.2. Ligand set

As absolute stereochemistry at C_2 position of Cassiarins is unknown, therefore we build both (*R*) and (*S*) stereoisomers, which were further minimised by MMFF94x Forcefield. Although, the energy minimisation step showed a reasonable energy difference between both the stereoisomer forms of individual Cassiarins (C, D, E & DBH), but these were used as such in our molecular modelling studies, as to avoid any pseudo positive or misleading results.

2.3. Molecular modelling

The proteins were prepared by, (a) removing of the water molecules from their crystal structures; (b) modelling the missing or breaks in their loops; and (c) protonation of the structure. Later, the co-crystallise ligand binding site or saved dummy atoms on proteins were used for docking of the Cassiarins. This inverse screening was performed by utilising 2 docking placement methods (also called, "Differential placement method based docking"). The first was the alpha triangle placement method, which generates the ligand-protein poses based on the overlapping of ligand atom triplets onto the triplets of protein point sites (are, also called alpha sphere centres). At each iteration cycle, a pose was determine based on sampling of a random triplet of ligand atoms over a random triplet of alpha sphere centres. The following setting was used for this method: minimum and maximum iterations cycles were set 800,000 and 5,000,000 respectively with timeout

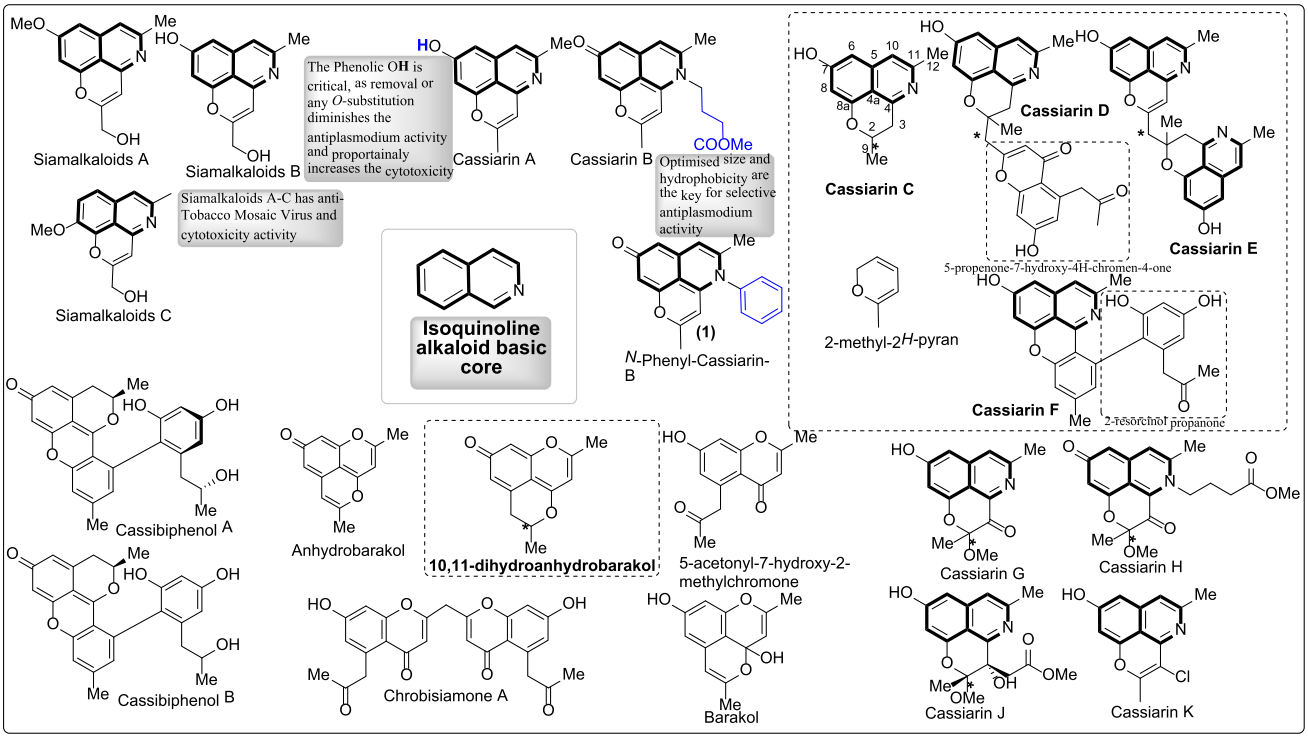

Fig. 1. Chemical structures of compounds isolated from *Cassia siamea* (Leguminosae).

(6000 s). The second was triangle matcher placement method, which generate the ligand-protein poses by aligning the ligand atoms triplet on triplets of alpha spheres in a more systematic way than in the Alpha Triangle method (method setting was, total number of returned poses was set 100,000, with time out 3000 s). Lastly, we utilised another approach which was different than the previous docking methods, i.e. grid based docking, as a part of VlifeMDS suite tool (VLife, 2010) which uses the genetic algorithm for grid formation and docking. Later, we compare the docking binding affinities, resulted from these methods, to get the confidence in prioritising the most putative Cassiarin targets.

3. Result and discussions

3.1. Protein set and docking

All the 1047 proteins were retrieved from protein data bank, which were found to belongs to 147 different protein-types. This protein dataset was divided into 2 categorises: one which has co-crystallise ligands and other one, without co-crystallise ligands. In case of co-crystallise ligand containing protein-types, we considered all those structures for a protein where co-crystallise ligand has a diverse chemotype in its structure. Later, we performed the self-docking to filter the most suitable protein crystal structure based on the min. RMSD value for its own co-crystallise ligand. In those protein-type, where protein structure does not contain any co-crystallise ligand, the structures were chosen based on their resolution (*Res.*). In order, to find the active site on those structure which does not contain co-crystallise ligand, active site finder tool was used to identify the active patches for the docking. Later, alpha triangle and triangle matcher placement methods resulted in various docking poses, which were ranked by GBVI/WSA *dG* scoring function (results for alpha triangle and triangle matcher are provided in Supplementary information, Table 1 and Table 2 respectively). While, the grid based docking results are enlisted in Supplementary information as Table 3. The grid based docking was performed on a larger area (80 × 80 × 80), as increased size of sheared active cavity results more conspicuous differences in the docking energies which could be useful in separating closely related putative targets.

The energy minimisation step revealed the most stable conformation among the isomers of individual Cassiarins, see in Table 3.

Table 1
Enlisting the *in vitro* antiplasmodial and cytotoxicity activities of natural compounds isolated from *Cassia siamea* plant.

Alkaloids	Plasmodium facliparum (IC50 = μM)	Cytotoxicity (μM)	Reference
Chloroquine	0.011[a]	36.1[c]	Morita et al. (2009)
Cassiarin A	0.023[a], 0.005[b]	>100[c], 35[e]	Morita et al. (2009, 2007)
Cassiarin B	22.0[a], 6.9[b]	>100[c], >100[e]	Morita et al. (2009, 2007)
Cassiarin C	24.2[a]	>100[d]	Oshimi et al. (2009)
Cassiarin D	3.6[a]	>100[d]	Oshimi et al. (2009)
Cassiarin E	7.3[a]	>100[d]	Oshimi et al. (2009)
10,11-dihydroanhydrobarakol (DHB)	2.3[a]	>100[d]	Oshimi et al. (2009)
Anhydrobarakol (ANH)	4.7[a], 7.8[a]	>100[d]	Oshimi et al. (2009, 2008)
5-acetonyl-7-hydroxy-2-methylchromone (AHMC)	8.6[a], 4.5[a]	>100[d]	Oshimi et al. (2009, 2008)
Chrobisiamone A	2.6[a]	–	Oshimi et al. (2008)
Cassiarin F	3.3[b]	>50[d]	Deguchi et al. (2011)

[a] Chloroquine-sensitive *P. falciparum* strain 3D7.
[b] *P. falciparum* 3D7.
[c] MCF7 (human breast adenocarcinoma) cell line.
[d] HL-60 Human blood premyelocytic leukaemia.
[e] P388 mouse leukaemia cells.

Table 2
The selected proteins with their PDB codes, resolution (Res.), co-crystallise ligand and self-docking RMSD values are provided in this table.

	Protein	PDB	Res. (Å)	Co-crystallized ligand	Min. RMSD values
1.	Dihydroorotate dehydrogenase	4CQ8	1.98	5-(4-Cyano-2-methyl-1*H*-benzimidazol-1-yl)-*N*-cyclopropylthiophene-2-carboxamide	0.406
2.	Triosephosphate Isomerase	1O5X	1.10	*Na*[f]	
3.	PfA-M1	3T8V	1.80	*N*-[(2-{2-[(*N*-{(2*S*,3*R*)-3-amino-4-[4-(benzyloxy)-phenyl]-2-hydroxybutanoyl}-L-alanyl) amino]ethoxy}ethoxy)acetyl]-4-benzoyl-L-phenylalanyl-N_6-hex-5-ynoyllysinamide	1.354
		4ZW3	1.80	*Tert*-Butyl [(1*S*)-1-(4-bromophenyl)-2-(hydroxyamino)-2-oxoethyl]-carbamate	1.080
		4X2U	1.50	Tosedostat	0.511
		4K5L	1.91	Phosphonic Arginine	1.160
		4R5X	1.85	3-amino-*N*-{(1*R*)-2-(hydroxyamino)-2-oxo-1-[4-(1H-pyrazol-1-yl)-phenyl]-ethyl}-benzamide	1.492
		3EBH	1.65	2-(3-Amino-2-hydroxy-4-phenyl-butyrylamino)-4-methyl-pentanoic acid	0.850
4.	PfA-M17	4ZY2	2.10	*N*-[(1*R*)-2-(hydroxyamino)-2-oxo-1-(3′,4′,5′-trifluorobiphenyl-4-yl)-ethyl]-2,2-dimethylpropanamide	1.001
		4X2T	2.73	Tosedostat	0.701
		3KR4	2.00	2-(3-Amino-2-hydroxy-4-phenyl-butyrylamino)-4-methyl-pentanoic acid	0.396
		4R76	2.50	3-Amino-*N*-{(1*R*)-2-(hydroxyamino)-2-oxo-1-[4-(1*H*-pyrazol-1-yl)-phenyl]-ethyl}-benzamide	0.612
		5CBM	2.30	(2*S*)-2-{[(*R*)-[(*R*)-amino(phenyl)-methyl]-(hydroxy)phosphoryl]-methyl}-4-methylpentanoic acid	0.807
		4K3N	2.00	{(*R*)-amino[4-(1*H*-pyrazol-1-yl)-phenyl]-methyl}-phosphonic acid	1.208
		3T8W	2.00	*N*-((2*R*,3*S*,6*S*,18*S*,21*S*)-2-amino-18-(4-benzoylbenzyl)-21-carbamoyl-3-hydroxy-6-(naphthalen-2-ylmethyl)-4,7,16,19-tetraoxo-1-phenyl-11,14-dioxa-5,8,17,20-tetraazapentacosan-25-yl)-hex-5-ynamide	1.409
		3Q43	1.8	N-[(2*S*,3R)-3-amino-2-hydroxy-4-(4-methoxyphenyl)-butanoyl]-L-leucine	0.815
5.	GMP synthetase	3UOW	2.72	Xanthosine-5′-monophosphate	0.704
6.	Enoyl-ACP Reductase	3LT0[b]	1.96	4-(2,4-dichlorophenoxy)-3-hydroxybenzaldehyde	0.560
		1ZXB	2.68	3-Chloro-4-(4-chloro-2-hydroxyphenoxy)-*N*-methylbenzamide	0.788
		1V35	2.50	Nicotinamide adenine dinucleotide (NADH)	0.818
		4IGE[b]	2.15	7-(4-Chloro-2-hydroxyphenoxy)-4-methyl-2H-chromen-2-one	0.551
		2NQ8	2.50	Isoniazid-Nicotinamide adenine dinucleotide (INH-NAD)	0.914
		1NHW	2.35	2-(2,4-Dichloro-phenylamino)-phenol	0.907
		2FOI	2.50	4-(2,4-Dichlorophenoxy)-2′-methylbiphenyl-3-ol	1.020
7.	Beta-Hydroxyacyl-Acyl Carrier Protein Dehydratase	3AZB	2.60	5-chloro-8-[(3-chlorobenzyl)-oxy]-quinoline	0.611
8.	Prolyl-tRNA synthetase	4OLF	2.90	Halofuginone	1.270
		4WI1	1.65	1-(4-fluorophenyl)-3-[4-(4-fluorophenyl)-1-methyl-3-(trifluoromethyl)-1H-pyrazol-5-yl]-urea	0.501
9.	PfHAD1	4ZEV	1.80	Mannose-6-Phosphate	0.323
10.	Spermidine synthetase	4BP3	1.75	Decarboxylated *S*-adenosyl-methionine	0.901
		3RIE	1.90	5′-deoxy-5′-methylthioadenosine	0.818
		2I7C	1.71	*S*-adenosyl-1,8-diamino-3-thiooctane	0.450
		2HTE	2.00	5′-deoxy-5′-methylthioadenosine	0.512
11.	CDPK4	4QOX	2.75	3-(3-bromobenzyl)-1-*tert*-butyl-1H-pyrazolo-[3,4-*d*]pyrimidin-4-amine	0.717
12.	CDPK2	4MVF	2.00	Staurosporine	0.825
13.	HSP90	3PEH	2.75	2-amino-4-{2,4-dichloro-5-[2-(diethylamino)-ethoxy]-phenyl}-*N*-ethylthieno[2,3-*d*]-pyrimidine-6-carboxamide	0.309
		3PEJ	2.81	Macbecin	0.532
		3K60	2.30	Adenosine diphosphate (ADP)	0.599
		3IED	2.01	Adenylyl-Imidodiphosphate (AMPPN)	1.402
14.	Fructose-1,6-bisphosphate aldolase	4TR9	2.11	*N*′-[(*E*)-(2,4-dichlorophenyl)-methylidene]-3,4-dihydroxybenzohydrazide	0.373
15.	Ferredoxin-NADP+ reductase	2OK8	2.40	Nicotinamide adenine dinucleotide phosphate (NADP)	1.007
		2OK7	2.70	Adenosine-2′-5′-Diphosphate (2'-ADP)	0.641
16.	Dihydrofolate reductase-thymidylate synthase (PfDHFR-TS)	1J3I	2.33	WR99210	0.513
		3UM8	2.6	Cycloguanil	0.998
		3QGT	2.3	Pyrimethamine	1.604
		3DGA	2.7	*N*-[2-chloro-5-(trifluoromethyl)-phenyl]imidodicarbonimidic diamide	1.200
		4DPD	2.5	Dihydrofolic acid	0.888
17.	D-aminoacyl-tRNA deacylase (DTD)	4NBI	1.86	3′-deoxy-3′-(D-tyrosylamino)-adenosine	0.711
		3LMV	2.83	4-(2-Hydroxyethyl)-1-piperazine ethanesulfonic acid	1.302
		3KO3	2.09	Adenosine triphosphate (ATP)	1.009
		3KO5	2.8	ADP	0.977
18.	FK506	4QT3	1.40	Rapamycin	0.221
		4J4N	2.75	N-(2-ethylphenyl)-2-(3H-imidazo[4,5-b]pyridin-2-ylsulfanyl)acetamide	0.708
		2VN1	2.35	8-Deethyl-8-[but-3-enyl]-ascomycin	0.890
19.	Lactate dehydrogenase	1T24	1.70	4-Hydroxy-1,2,5-oxadiazole-3-carboxylic acid	0.901
		1XIV	1.70	2-({4-Chloro-2-[hydroxy(methoxy)methyl]cyclohexyl}amino)ethane-1,1,2-triol	0.990
		1CET	2.05	Chloroquinein[e]	1.313
		1LDG	1.74	NADH	1.607
		4B7U	1.88	Bicine	0.780
20.	PfPK5	1V0O	1.90	Indirubin-5-sulphonate	0.449
21.	Plasmepsin II	1LF2	1.80	3-amino-*N*-{4-[2-(2,6-dimethyl-phenoxy)-acetylamino]-3-hydroxy-1-isobutyl-5-phenyl-pentyl}-benzamide	0.760
		4CKU	1.85	5-[1,1-bis(oxidanylidene)-1,2-thiazinan-2-yl]-N3-[(2*S*,3R)-4-[2-(3-methoxyphenyl)propan-	0.831

(*continued on next page*)

Table 2 (*continued*)

	Protein	PDB	Res. (Å)	Co-crystallized ligand	Min. RMSD values
				2-ylamino]-3-oxidanyl-1-phenyl-butan-2-yl]-N_1,N_1-dipropyl-benzene-1,3-dicarboxamide	
		2BJU	1.56	*N*-(*R*-carboxy-ethyl)-α-(*S*)-(2-phenylethyl)	0.451
		2IGX	1.70	5-Pentyl-*N*-{[4′-(piperidin-1-yl-carbonyl)biphenyl-4-yl]methyl}-*N*-[1-(pyridin-2-ylmethyl) piperidin-4-Yl]pyridine-2-carboxamide	1.222
22.	Plasmepsin I	3QS1	3.10	KNI-10,006	0.619
23.	Plasmepsin IV	1LS5	2.80	Pepstatin A	0.870
24.	Phosphoglycerate Kinase	1LTK	3.00	AMP	0.391
25.	Glutathione reductase	1ONF	2.60	Flavin Adenine Dinucleotide (FAD)	0.904
26.	Thymidylate Kinase	2YOG	1.50	1-[4-Chloranyl-3-(trifluoromethyl)-phenyl]-3-[[(2*R*,3*S*)-5-[5-methyl-2,4-*bis*-(oxidanylidene)pyrimidin-1-yl]-3-oxidanyl-oxolan-2-yl]methyl]thiourea	0.60
		2WWF	1.89	ADP	0.832
27.	Ubiquitin Carboxyl-Terminal Hydrolase 3 (Uchl3)	2WDT	2.30	*Na*[f]	
28.	Purine Nucleoside Phosphorylase	2BSX	2.00	Inosine	0.456
		1Q1G	2.02	3,4-Dihydroxy-2-[(methylsulfanyl)methyl]-5-(4-oxo-4,5-dihydro-3H-pyrrolo [3, 2-*d*] pyrimidin-7-yl)pyrrolidinium	0.702
29.	Histo-Aspartic Protease (Hap)	3QVI	2.50	KNI-10,395	0.315
30.	Purine Phosphoribosyltransferase	1CJB	2.00	(1*S*)-1(9-deazahypoxanthin-9-yl)1,4-dideoxy-1,4-imino-D-ribitol-5-phosphate	0.611
		3OZG	1.99	[(3*S*)-4-Hydroxy-3-{[(4-oxo-4,5-dihydro-3H-pyrrolo[3,2-d]pyrimidin-7-yl)methyl]amino} butyl]phosphonic acid	0.942
31.	Peptide Deformylase	1RL4	2.18	2-{*N*′-[2-(5-amino-1-phenylcarbamoyl-pentylcarbamoyl)-hexyl]-hydrazinomethyl}1.4-hexanoic acid-(5-amino-1-phenylcarbamoyl-pentyl)-amide	0.664
32.	Cyclophilin	1QNG	2.10	Cyclosporin A	0.782
33.	Glutathione-S-Transferase	4ZXG	1.70	Ligandin	0.560
34.	Glyceraldehyde-3-Phosphate Dehydrogenase	1YWG	2.60	Nicotinamide Adenine Dinucleotide (NAD)	1.104
35.	Ribose 5-phosphate isomerase	2F8M	2.09	*Na*[f]	
36.	MTIP	4R1E	1.98	5-{[(2-aminoethyl)-sulfanyl]methyl}furan-2-carbaldehyde	0.309
37.	Guanylate Kinase	1Z6G	2.18	4-(2-Hydroxyethyl)-1-piperazine ethanesulfonic acid	0.655
38.	ARO (armadillo repeats only protein)	5EWP	1.80	*Na*[f]	
39.	cGMP-dependent protein kinase	4OFG	2.0	Cyclic Guanosine Monophosphate (cGMP)	0.831
40.	Apical membrane antigen 1	4Z0E	1.9	*Na*[f]	
		4R19	1.8	*Na*[f]	
41	DXR	5JAZ	1.4	[(2*R*)-2-{2-[hydroxy(methyl)amino]-2-oxoethyl}-5-(naphthalen-1-yl)pentyl]phosphonic acid	0.561
		4Y67	1.6	[(2*R*)-2-{2-[hydroxy(methyl)amino]-2-oxoethyl}lo-5-phenylpentyl]phosphonic acid	0.410
		4KP7	2.0	[(*S*)-({2-[hydroxy(methyl)amino]-2-oxoethyl}sulfanyl)(phenyl)methyl]phosphonic acid	0.701
		3WQR	1.97	[(1*S*)-4-[hydroxy(methyl)amino]-1-(4-methoxyphenyl)-4-oxobutyl]phosphonic acid	0.809
		4GAE	2.30	[(1*S*)-3-[acetyl(hydroxy)amino]-1-(pyridin-4-yl)propyl]phosphonic acid[e]	0.677
				[(1*R*)-3-[acetyl(hydroxy)amino]-1-(pyridin-4-yl)propyl]phosphonic acid[e]	0.719
		3AU9	1.90	3-[formyl(hydroxy)amino]propylphosphonic acid	0.884
42.	kelch protein	4YY8	1.81	*Na*[f]	
43.	Pf41	4YS4	2.45	*Na*[f]	
44.	Pf12	2YMO	1.90	*Na*[f]	
45.	PfGrx1	4MZB	1.04	3-[*N*-morpholino]-propane sulfonic acid	0.698
46.	Tryptophanyl-tRNA synthetase	4JFA	2.60	Tryptophan	1.019
		4J75	2.40	Tryptophanyl-5′-AMP	0.719
47.	Tyrosyl-*t*RNA Synthetase	3VGJ	2.21	Tyrosyl-AMP	1.102
48.	Phosphoethanolamine Methyltransferase	4FGZ	1.99	Amodiaquine	0.359
		3UJB	1.52	*S*-adenosyl-L-homocysteine	0.902
49.	MIF	2WKF	2.05	*Na*[f]	
50.	Peroxiredoxin	4D73	1.80	*Na*[f]	
51.	Glycerol-3-Phosphate Dehydrogenase	1YJ8	2.85	*Na*[f]	
52.	6-Pyruvoyl Tetrahydropterin Synthase (PTPS)	1Y13	2.20	Biopterin	0.772
53.	Phosphoglycerate Mutase	3EOZ	2.40	*Na*[f]	
54.	Diadenosine Triphosphate Hydrolase	5CS2	1.65	Cyclomarin A	0.490
55.	Aspartate Transcarbamoylase	5ILQ	2.50	*Na*[f]	
56.	Plasmodium Falciparum Rab6	1D5C	2.30	Guanosine Diphosphate (GDP)	0.705
57.	Acyl-COA Binding Protein	1HBK	2.00	Coenzyme A	0.667
58.	Pfg27	1N81	2.10	*Na*[f]	
59.	Fab Complex Whith Plasmodium Falciparum Msp1-19	1OB1	2.90	*Na*[f]	
60.	Adenylosuccinate synthetase	1P9B	2.00	6-Phosphoryl-Inosine Monophosphate	0.443
61.	Nucleoside diphosphate kinase B	1XIQ	3.05	*Na*[f]	
62.	D-Ribulose 5-Phosphate 3-Epimerase	1TQX	2.00	*Na*[f]	
63.	GTPase Rab6	1D5C	2.30	GDP	0.548
64.	GTPase Rab11	3BFK	1.80	GDP	1.001
65.	Rab5 protein	3CLV	1.89	GDP	0.670
66.	RabGDI	3P1W	1.85	*Na*[f]	
67.	Orotidine 5′-Monophosphate Decarboxylase	3VI2	2.10	4-(2-hydroxy-4-methoxyphenyl)-4-oxobutanoic acid	0.487

Table 2 (*continued*)

	Protein	PDB	Res. (Å)	Co-crystallized ligand	Min. RMSD values
		2Q8Z	1.8	6-Amino-UMP	0.861
		3S9Y	1.7	6-amino-5-fluorouridine 5′-(dihydrogen phosphate)	0.914
		2ZA1	2.65	Orotidine 5′-monophosphate	0.503
68.	Oxoacyl-Acp Reductase	2C07	1.50	*Na*[f]	
69.	ClpP protease catalytic domain from Plasmodium falciparum	2F6I	2.45	*Na*[f]	
70.	Glutamate Dehydrogenase	2BMA	2.70	*Na*[f]	
71	glutamate dehydrogenase 2	3R3J	3.10	*Na*[f]	
72.	PHIST	4JLE	2.35	*Na*[f]	
73.	PF3D7_0823300 (GCN5)[a,c]	4QNS	1.50	*Na*[f]	
	Histone acetyltransferase GCN5	5TPX	2.10	(1S, 2S)-N_1, N_1-dimethyl-N_2-(3-methyl-[1,2,4]triazolo[3,4-*a*]phthalazin-6-yl)-1-phenylpropane-1,2-diamine	0.799
74.	PFA0510w (Bromodomain protein)[a]	4PY6	2.50	*Na*[f]	
75.	PF3D7_1475600	4NXJ	2.18	*Na*[f]	
76.	PF10_0328	3FKM	2.50	*Na*[f]	
77.	Ubiquitin conjugating enzyme UBC9	4M1N	1.50	*Na*[f]	
78.	Ubiquitin conjugating enzyme E2	2H2Y	2.80	*Na*[f]	
79.	Ubiquitin carrier protein	2R0J	1.85	*Na*[f]	
80.	Ubiquitin conjugating enzyme e2[a]	2Q0V	2.40	*Na*[f]	
81.	PF10_0330 (Ubiquitin-conjugating enzyme)[a]	2ONU	2.38	*Na*[f]	
82.	Falcilysin (protein)	3S5M	1.55	*Na*[f]	
83.	Calcium-dependent protein kinase 3	3 K21	1.15	*Na*[f]	
84.	Calcium-dependent protein kinase[a]	3MSE	2.10	*Na*[f]	
85.	Pyruvate kinase	3KHD	2.70	*Na*[f]	
86.	Calcium-dependent protein kinase 2	3PM8	2.00	*Na*[f]	
87.	ADP-Ribosylation Factor 1	3LRP	2.50	GDP	0.758
88.	Aspartate Aminotransferase	3K7Y	2.80	Pyridoxal phosphate (PLP)	1.009
89.	PFC0360w protein (HSP90 Activator protein)	3NI8	2.50	*Na*[f]	
90.	MAP-2 kinase	3NIE	2.30	Phosphoaminophosphonic acid-adenylate ester	0.417
91.	Serine/threonine kinase-1	3LLT	2.50	Phosphoaminophosphonic acid-adenylate ester	0.857
92.	Ornithine delta-aminotransferase	3LG0	2.30	*Na*[f]	
93.	Aha-1	3N72	1.77	*Na*[f]	
94.	Arginase	3MMR	2.14	2(*S*)-amino-6-boronohexanoic acid	0.637
		3SL1	1.90	6-(dihydroxyboranyl)-2-methyl-L-norleucine	1.377
95.	Malarial Clpb2 Atpase/Hsp101 Protein	4IRF	1.65	*Na*[f]	
96.	ClpB protein (Green fluorescent protein)[a]	4XBI	1.80	*Na*[f]	
97.	Maltose-binding periplasmic protein	4O2X	2.70	*Na*[f]	
98.	Aquaglyceroporin	3C02	2.05	*β*-Octylglucoside	1.110
99.	Profilin	2JKG	1.89	*Na*[f]	
100.	Microtubule-associated protein 1 light chain 3	4EOY	2.22	*Na*[f]	
101.	Thrombospondin related anonymous protein	4F1J	1.73	*Na*[f]	
102.	Apicoplast TIC22[a]	4E6Z	2.15	*Na*[f]	
103.	Diphenyl Nucleoside	3T64	1.65	2′, 5′-Dideoxy-5′-[(diphenylmethyl)amino]-uridine	0.598
		2Y8C	2.10	5′-Tritylated Deoxyuridine Analogue	0.617
104.	Erythrocyte Binding Antigen Region II Region 175	4K2U	2.25	*Na*[f]	
		1ZRO	2.25	α-2,3-sialyllactose	0.896
		1VYQ	2.40	2,3-deoxy-3-fluoro-5-*O*-trityluridine	1.006
105.	Erythrocyte Membrane Protein 1	3CPZ	2.80	*Na*[f]	
106.	Erythrocyte Binding Antigen 140	4JNO	3.00	*O*-sialic acid	1.017
107.	Dbl6 Epsilon Domain (VAR2CSA)	2Y8D	1.84	*Na*[f]	
		2XU0	2.06	*Na*[f]	
108.	MSPDBL2	3VUU	2.09	*Na*[f]	
109.	Erythrocyte Membrane Protein-1 (PfEMP1) variant 2 of strain MC	3C64	2.40	*Na*[f]	
110.	2C-methyl-D-erythritol-2,4-cyclodiphosphate synthase (IspF)	4C81	1.56	Cytidine-5′-diphosphate	1.308
111.	Thioredoxin reductase	4J56	2.37	FAD	1.100
112.	Thioredoxin-2	4O32	2.20	*Na*[f]	
113.	Thioredoxin Peroxidase 2	2C0D	1.78	*Na*[f]	
114.	Peroxiredoxin	1XIY	1.80	*Na*[f]	
115.	Thioredoxin like protein[a]	3CXG	2.00	*Na*[f]	
116.	Thioredoxin like protein[a]	1SYR	2.95	*Na*[f]	
117.	Peptidase[a]	5JR6	2.30	*Na*[f]	
118	ATP-dependent Clp protease	4GM2	2.80	*Na*[f]	
119	GAP50	3TGH	1.70	*Na*[f]	
120.	Tumor protein (TCTP)	3P3K	2.55	*Na*[f]	
121.	ARF GTPase activating protein	3SUB	2.40	*Na*[f]	
122.	Sir2A	3U31	2.20	NAD	0.709

(*continued on next page*)

Table 2 (*continued*)

	Protein	PDB	Res. (Å)	Co-crystallized ligand	Min. RMSD values
123.	Ser/Thr protein kinase	2PMO	2.90	Hymenialdisine	0.993
124.	Adenylate Kinase	3TLX	2.75	ADP	0.989
		1CJB	2.00	(1*S*)-1(9-Deazahypoxanthin-9yl)1,4-dideoxy-1,4-imino-d-ribitol-5-phosphate	0.640
		2VFA	2.80	Guanosine Monophosphate (GMP)	1.082
125.	Apicomplexan AP2 protein	3IGM	2.40	*Na*[f]	
126.	Nucleosome assembly protein 1[a]	3FS3	2.30	*Na*[f]	
127.	Nucleosome assembly protein	3KYP	2.80	*Na*[f]	
128.	Falcipain (*Isoform-2*) (*Isoform-3*)[d]	3BPF	2.90	*N*-[*N*-[1-Hydroxycarboxyethyl-carbonyl]leucylamino-butyl]-guanidine	0.613
		3BWK	2.43	*N*-2-(Morpholin-4-ylcarbonyl)-*N*-[(3*S*)-1-phenyl-5-(phenylsulfonyl)pentan-3-yl]-L-leucinamide	0.706
129.	Glycerol Kinase	2W41	2.41	ADP	0.83
130.	Malaria Sporozoite Protein Uis3[a]	2VWA	2.50	Phosphatidylethanolamine	1.502
131.	EBA-175 region VI	2RJI	1.80	*Na*[f]	
132.	Pyrroline carboxylate reductase	2RCY	2.30	NADP	0.906
133.	Phosphatidylethanolamine-Binding Protein	2R77	1.60	*Na*[f]	
134.	Internal Kinesin	1RY6	1.60	*Na*[f]	
135.	Dynein Light Chain 1	1YO3	1.65	*Na*[f]	
136.	Malarial Hypothetical protein	1ZSO	2.17	*Na*[f]	
137.	Adenosyl-homocysteinase	1V8B	2.40	NAD	1.205
138.	Fe-Superoxide Dismutase	2GOJ	2.00	*Na*[f]	
139.	Ribosomal RNA Methyltransferase[a]	2PLW	1.70	*S*-Adenosyl-L-homocysteine (SAM)	0.666
140.	Protein-L-isoaspartate *O*-methyltransferase *β*-aspartate methyltransferase	2PBF	2.00	SAM	0.480
141.	Dimethyladenosine transferase[a]	2H1R	1.89	*Na*[f]	
142.	Plasmodial PLP Synthase	2ABW	1.62	Tetraethylene glycol	0.922
143.	Actin Depolymerizing Factor	3Q2B	1.60	D(-)-tartaric acid	0.801
144.	Glucose-6-phosphate isomerase	3PR3	2.45	Fructose-6-phosphate	0.442
145.	Methionine aminopeptidase	3S6B	1.95	*Na*[f]	
146.	Nucleolar GTP-binding protein 1[a]	2QU8	2.01	GDP	0.575
147.	Orotate Phosphoribosyl transferase	4FYM	2.60	*Na*[f]	

[a] Putative.
[b] Both have close self-docking RMSD.
[c] Pairwise Sequence alignment shows PF3D7_0823300 (GCN5) ¥ is a Histone acetyltransferase (GCN5).
[d] It is isoform-3 of Falcipain and has identity of ~66%.
[e] co-crystallise ligand is in racemic mixture.
[f] Na: no co-crystal ligand. Res. = Resolution of crystal structure.

Table 3
Energy profile of stereoisomers of Cassiarins isoforms.

	R-Cassiarins C	*S-Cassiarins* C	R-Cassiarins D	S-Cassiarins D	R-Cassiarins E	S-Cassiarins E	*R-DHB*	*S-DHB*	Cassiarins F
Stretch (E_{Str})	0.8104	0.8429	2.9064	2.9917	1.9958	2.0769	0.9461	0.9461	2.4203
Bend (E_B)	2.7384	3.0206	9.1569	9.3554	6.0665	6.2631	2.8678	2.8678	7.9539
Stretch-Bend ($E_{Str\text{-}B}$)	0.0803	0.1062	0.3036	0.3219	0.1787	0.1957	−0.0318	−0.0318	−0.0135
Torsion (E_{tor})	−8.4023	−7.9008	−12.7333	−12.5845	−17.7278	−17.5754	−4.5516	−4.5516	0.0139
Non-1,4 VDW (E_{nVDW})	−3.9005	−3.9103	−5.2953	−5.4962	−8.6554	−8.8469	−3.4075	−3.4075	−12.0544
1,4 VDW (E_{VDW})	15.9754	15.8132	30.3389	30.4761	32.8734	33.0109	16.7451	16.7451	28.1042
Dipole/Dipole ($E_{d\text{-}d}$)	0.2167	0.2191	−1.3802	−1.2855	−0.3444	−0.3346	−0.1735	−0.1735	−0.4288
Total Energy (E = kcal/mol)	7.5183	8.1907	23.2970	23.7788	14.3868	14.7896	12.3946	12.3946	25.9957

Total Energy $_{(MM2)} = E_{Str} + E_B + E_{Str\text{-}B} + E_{tor} + E_{nVDW} + E_{VDW} + E_{d\text{-}d}$.

In general, we found that *R*-stereoisomers have more energy minimised structures than their *S*-isoforms and DHB stereoisomers appeared to be unaffected with the C_2-stereochemistry. The large structure containing isoforms show more energy penalties than their smaller isoforms, as follow: F > D > E > DHB > C, which seems reasonably obvious, as these have more steric hindrance in their structures. Also, we found certain isoforms consist similar structural connectivity but shows significant differences in their energy levels (*C vs* DHB; E *vs* D), indicating that the subtle alteration, like replacing of nitrogen as from N_1_isoquinoline by oxygen, diminishes the aromatic character, which increases the cyclic ring constrain.

Based on the binding energies, resulted from three different docking placement methodologies, we considered and compare top 25 most energy minimised Cassiarin-protein complexes and selected only those ones which were present in the result of all three docking methods (Table 4 in Supplementary information). Based on these observations, we found 16 targets as for individual Cassiarin stereoisomer, listed in Table 4. While Table 5, summarises the basic structural features of these targets. The binding mode of Cassiarins with these protein targets has been discussed descriptively in the later sections of this article.

3.2. Tryptophanyl-tRNA synthetase

The cytosolic tryptophanyl-tRNA synthetase of *Plasmodium falciparum* (*Pf*-cTrpRNA, PDB: 4J75, *Res.*2.4 Å, (Koh et al., 2013))

Table 4
The most common PDBs as targets were identified for Cassiarins isoforms/isomers.

R-Cassiarins C	*S*-Cassiarins C	R-Cassiarins D	S-Cassiarins D	R-Cassiarins E	S-Cassiarins E	*R*-DHB	*S*-DHB	Cassiarins F
4J75	4J75	2W41	5EWP	3UOW	3LG0	3VGJ	1P9B	4j75
3VGJ	3VGJ	3PR3	2W41	3FS3		4Y67	3FS3	4Y67
3MMR	3MMR	3VUU	4Y67	2W41		1P9B	3MMR	
4Y67	4YY8			4YY8		4J75	4J75	
				2C07		3S6B	4Y67	
				3LT0		3PR3		

belongs to aminoacyl tRNA synthetase (aaRSs) class, which charges amino acids to their cognate tRNAs during protein synthesis and requires a large conformational change during their functioning. Previous studies on bacterial and human *t*RNA synthetase revealed key structural features: (a) In bacteria, these have open, ligand-free state (F-state) where either Trptophan (Trp) or ATP can bind; (b) Simultaneous binding of Trp and ATP in the pre-transition state requires a conserved loop, KMSKS (^{492}K^{493}M^{494}S^{495}S^{496}T in *P. falciparum* and ^{349}K^{350}M^{351}S^{352}A^{353}S in humans) (Datt and Sharma, 2014) to close onto the active site and *C*-terminal domain moves toward the active site, containing Rossmann-fold domain; (c) After the intermediate tryptophanyl-adenylate (WAMP) formation, both the KMSKS loop and *C*-terminal domain move slightly away from the catalytic core to allow to release of the product (called, as P-state) (Datt and Sharma, 2014) (d) While in human cytoplasmic TrpRS (*Hs-c*TrpRS), the binding of Trp is mainly accompanied by the *N*-terminus and a conserved AIDQ motif. Phylogenetically, *Pf-c*TrpRS is more close to *Hs-c*TrpRS (∼44% identity) than the human mitochondrial TrpRS (∼16% identity) (Koh et al., 2013).

According to literature (Datt and Sharma, 2014), the WAMP binds to the 28 key amino acid residues of *Pf-c*TrpRNA (highlighted as bold single letter amino acid code): (i) ^{296}**YTGR**^{300}**G** and ^{317}**H**X**GH**X**I**^{323}P in the tip of a loop between β_3 and α5 (ii) ^{341}**Q**X**S**XX**EK** (iii) ^{415}**Y**XXX^{419}**Q** (iv) ^{450}**VPQG**X**D**^{456}**Q**XXX^{460}**F** (v) ^{481}**VF**^{483}**M** (vi) ^{492}**K**^{493}**M**, as shown in Fig. 2(A) and as follow: (a) The indole and adenine ring has π-π interactions with Tyr306, Phe482; (b) The free NH_2 and N_1-heteroatom of adenine ring has *H*-bond interaction with backbone of Met483; (c) The hydroxyl (*OH*) groups of ribose sugar shows *H*-bonding with β-COOH of Asp455 and backbone of Glu452; (d) The phosphate head lies within *H*-bond distance with side chain of Arg309 and backbone of Gly310; (e) The NH_2 tethered functionality of tryptophan interacts with Gln429. Like adenine ring of WAMP, tetracyclic core of Cassiarin-F (Orange) faces vertically to the β_7-strand region extended from ^{481}Val to ^{496}Thr and α_5-helix from ^{318}Leu to ^{334}Phe and also, has T-shaped π-π interactions with Phe482 (3.89 Å) and His320 (3.23 Å) (Sinnokrot and Sherrill, 2004), see in Fig. 2(B). The N_1-isoquinoline of tetracyclic ring of Cassiarin-F faces towards a cavity consist β_6-strand (region from ^{448}Cys to ^{453}Gly), ^{453}GID^{456}Q conserved motif, α_{11}-helix (region from ^{456}Q to ^{470}M) and has *H*-bond acceptor interaction with NH_2 terminus of the side chain of Gln456 (3.02 Å). The resorcinol phenolic-O*H* inclined towards the β_4-strand (region from ^{337}Pro to ^{342}Leu), α_6-helix (^{343}Ser to ^{350}Phe), showing *H*-bond donor interaction with γ-*COOH* acid side chain of Glu346 (2.43 Å). The extended propanone functionality aligned with β_3-strand (^{304}Tyr to ^{309}Arg), has *H*-bond acceptor interaction with guanidine side chain of Arg309 (1.95 Å) and amide backbone of Gly310 (2.09 Å). While the tricyclic ring of *R*-Cassiarin-C shows reverse orientation: (a) phenolic ring fitted into a pocket surrounded by α_{11} (region from ^{456}Q to ^{470}M) and conserved motif GIDQ, showing *H*-bond donor interactions with alcoholic side chain of Thr307 (2.39 Å; β3 strand) and amide backbone of Pro451 (2.39 Å; β_6: ^{448}Cys to ^{453}Gly), while its N_1-isoquinoline ring projected outwards, as shown in Fig. 2(C). Although, the *S*-isomer of Cassiarin-C attained a reasonable conformational binding change, as phenolic O*H* projected towards the α_6-helix and involved with γ-COOH group of Glu346 (2.32 Å), but its N_1-isoquinoline ring has *H*-bond acceptor interaction with Thr307 (2.76 Å) of β_3-strand and utilisation of conserved motif GIDQ, shows similar binding pocket like *R*-isomer-C, shown in Fig. 2(D). The heteroatom (N_1) replacement with oxygen atom in Cassiarin-C, brings *R*-DHB, which restricted the phenolic ring, aromatic character due to formation of quinone ring and also affected its binding with *Pf-c*TrpRNA. However, its binding resembles to the 2-resorcinol propanone substructure of Cassiarin F binding, as the carbonyl (C*O*) of quinone utilises ε-NH_2 of Lys347 (2.48 Å) of β_6-strand and have proximity with the conserved motif GIDQ, α_{11}, α_6 and β_3, as shown in Fig. 2(E). Although, as it is devoid of tetracyclic ring like in Cassiarin-F therefore the interactions with of β_7 region and α_5 got disappeared. The *S*-DHB has shown a close identity in its binding pattern like *R*-DHB, which would therefore similarly mimic interactions as like 2-resorcinol propanone of Cassiarin F, with slight variation in its binding conformation as resulted by the modification of C_2-stereochemistry, see in Fig. 2(F). The close binding behaviour of both isomers of DBH with regards to the 2-resorcinol propanone of Cassiarin-F, offers a possible bioisostere substitution on tetracyclic core of Cassiarin-F in order, to improve structure based rational design against *Pf-c*TrpRNA protein in *P. falciparum*. Additionally, we observed that *S*-DHB binding within the π-stacking interaction to the Tyr425 residue, which is deleted in human aminoacyl tRNA synthetase proteins and can be utilised as a structural feature in optimisation of NCE.

3.3. Tyrosyl-tRNA synthetase

Tyrosyl-tRNA synthetase (PDB: 3VGJ, *Res*. 2.21 Å, (Bhatt et al., 2011) belongs to the aminoacyl tRNA synthetase family proteins and therefore have similar function and catalytic motifs as seen in previous case of *Pf-c*TrpRNA, except its utilisation of tyrosine at the place of tryptophan, in the form of tyrosyl-AMP. It consists of a catalytic domain region started from residues 18–260, contains KMSKS and GIDQ conserved motifs. Also, as obvious, its nucleoside binding pocket interactions are similar like *Pf-c*TrpRNA (Fig. 3(A)), as (a) adenosine ring fits in the cavity constituted by Lys247, Leu238, Met 237, Gly236 and Met248 of complimentary K^{247}M^{248}SKS conserve domain (Fig. 3(B)); (b) The His70, Ala72 and Gln73 which lies at the tip of loop between α_1-helix/β_3-stand and Leu206, Asp209, Gln2010 of evolutionary conserved residues ^{207}GI^{209}D^{2010}Q create its sugar binding pocket; (c) Asp61, Phe63, Glu64 encloses the sugar-phosphate junction and phosphate head; (d) The Gln192, Asp195 located on the top of ionised NH_2 of tyrosine where the Trp94, Ala96, Ph99 composed hydrophobic pocket in order to accommodate aromatic phenol ring.

The molecular docking of *R*-Cassiarin-C has shown *H*-bond donor interactions with Thr307 and Gln452 through its phenolic (O*H*) group, as shown in Fig. 4(A). As compared to *R*-isomer, *S*-Cassiarin-C shows more suitability for AMP binding pocket, as: (a) its phenolic (OH) orientated similarly like phosphate heads and has *H*-bond acceptor-donor interactions with side chain of Lys77 (2.72 Å) and free COOH terminus of Arg61 (2.67 Å), (b) The

Table 5
Summary of individual protein target.

PDB	Protein/Target	Co-crystallise ligand	Structural features and functions
4J75	Tryptophanyl-tRNA synthetase	Trptophanyl-Adenosine monophosphate (WAMP)	• Utilises tryptophan as substrate • Contain 632 amino acids • Has KMSKS conserved loop and AIDQ motif in its active binding site
3VGJ	Tyrosyl-tRNA synthetase	Tyrosyl-Adenosine monophosphate (YAMP)	• Utilises tyrosine as substrate • Catalytic domain contains 18-260 amino acid residues • Has KMSKS conserved loop and AIDQ motif in its binding site
4Y67	1-Deoxy-*D*-Xylose-5-phosphate reductoisomerase	Fosmidomycin	• Homodimer in its active form • Each monomer is made up of two large domains • One large domain for NADPH • Other one for catalysis • FOSMIDOMYCIN inhibitors are most studied class
2W41	Glycerol kinase	Adenine Diphosphate	• Utilises glycerol as substrate • Participate in rate-limiting step in glycerol utilisation • Has 501 amino acid residues • Contains two domains separated by a deep cleft • Domain I (regions 1–262 and 436–471) • Domain II (regions 263–435 and 472–501) • Domain 1 is for glycerol binding; Domain II is for ADP binding. • Its kinase domain shows typical *H*-bond acceptor–donor triad interactions
3MMR	*Plasmodium falciparum Arginase*	2-(*S*)-amino-6-boronohexanoic acid	• Utilises binuclear manganese • Forms tetrahedral geometry with both the manganese atoms. • Close to human arginase I (28%) and II (27%)
3FS3	*Nucleosome Assembly Protein*	*n. a*	• 347amino acid long-dimer • Has two domains, domain I (mainly contain, dimerization helix-2, region started from 37 to 87) • Domain II, containing multiple α-helices and a subdomain containing four antiparallel β-strands (residues 128–185)
1P9B	*Adenylosuccinate synthetase*	GDP and IMP	• Consists of 19 strands (β_1–β_{19}), 12 α-helices and seven 3_{10} helices • It has nine parallel β-strands, with a tenth antiparallel strand (β_{19}) form a central sheet. • Has 4 subdomains • Subdomains III (residues 278–302) majorly constitute ligand binding pocket • It has 2 binding sites: orthosteric (IMP binding site) and allosteric (GTP binding site).
3PR3	*Glucose-6-Phosphate Isomerase*	Fructose-6-phosphate	• Orthosteric site contains key amino acids, Glu380, Lys540, Thr233, Lsy232, Thr236, Ser231 and Gly158 • Like, human glucose-6-phosphate isomerase (*Hs*G6PI), it also has two globular domains (as large and small domains) and an "arm-like" *C*-terminal tail
4YY8	*Kelch Motif Associated Protein of Plasmodium Falciparum*	Mono-alkylated *p*-substituted sulphonamides	• Made up of 28 β-strands where β_4 to β_{28} involved in the formation of its 6 kelch motifs • Every motif contains 4 β-strands in common, • 6 kelch motifs together built a propeller architecture
3LG0	*Ornithine δ-aminotransferase of Plasmodium falciparum (PfOAT)*	*n. a*	• Enzymatically active as a homodimer • High percentage of conserved residues in the active cavity, which is proximal to the interface between two subunits • Each subunit contains a pyridoxal-phosphate (PLP) binding domain and a substrate binding domain • PLP binding loop domain (region started from 287 to 293) and strictly conserved in all species
3LT0	*Enoyl Acyl Carrier Protein Reductase*	Triclosan and NADPH	• With its most studied class of inhibitor (triclosan derivatives), it shows formation of typically ternary complex of *Pf*ENR-NAD^+-triclosan • Ring A of Triclosan binds to hydrophobic pocket and has π-stacking interaction distance with nicotinamide ring of the cofactor NAD^+
2C07	*Oxoacyl Acyl-Carrier-Protein Reductase*	Triclosan and NADPH	• Most studies limited to triclosan and its derivatives. • Our comparative structural studies with *E.* coli found 4 key mutations: Ser99 (Gly41 in *E. coli*), Ser94 (Ala36 in *E. coli*), Arg95 (Thr37 in *E. coli*) and Ser198 (Gly137 in *E. coli*).
5EWP	*Armadillo Repeats Only Protein of Plasmodium Falciparum*	*n. a*	• 252 amino acid residues long dimer • Contains 15 α-helixes, form a characteristic alpha solenoid structure • Each Armadillo repeat is composed of a pair of alpha helices that form a hairpin structure
3S6B	*Methionine Aminopeptidase 1b*	*n. a*	• Comparative studies with human homologous protein: Thr156 and Ser268 mutated in place of Pro192 and Cys301 (in human),
3UOW	*Guanosine monophosphate synthetase*	Xanthose Monophosphate (XMP)	• It is dimeric in nature. • Each monomer is composed of two catalytic domains, an *N*-terminal independent GATase (1–236) and a *C*-terminal ATPPase domain (237–555) • Its dimer form is highly required for its activity as the interface has 108*C*-terminal residues of the ATPPase domain. • In this interface, two *cis*-prolines (Pro548–Pro549) allow a tetrahedral configuration of Asp543, Thr551, Glu553 and Arg539
3VUU	Merozoite surface proteins have erythrocyte-binding Duffy Binding Like Domains (*MSPDBL2)*	*n. a*	• Assist parasite for its initial binding to the surface receptors on the host red blood cell. • Consist of a boomerang shaped α-helical core formed from three subdomains • Subdomain 1 (region 161–225) only contains a 5-residue long α-helix (helix 1) provide a junction for subdomains 2 and 3

n.a. no crystallise protein.

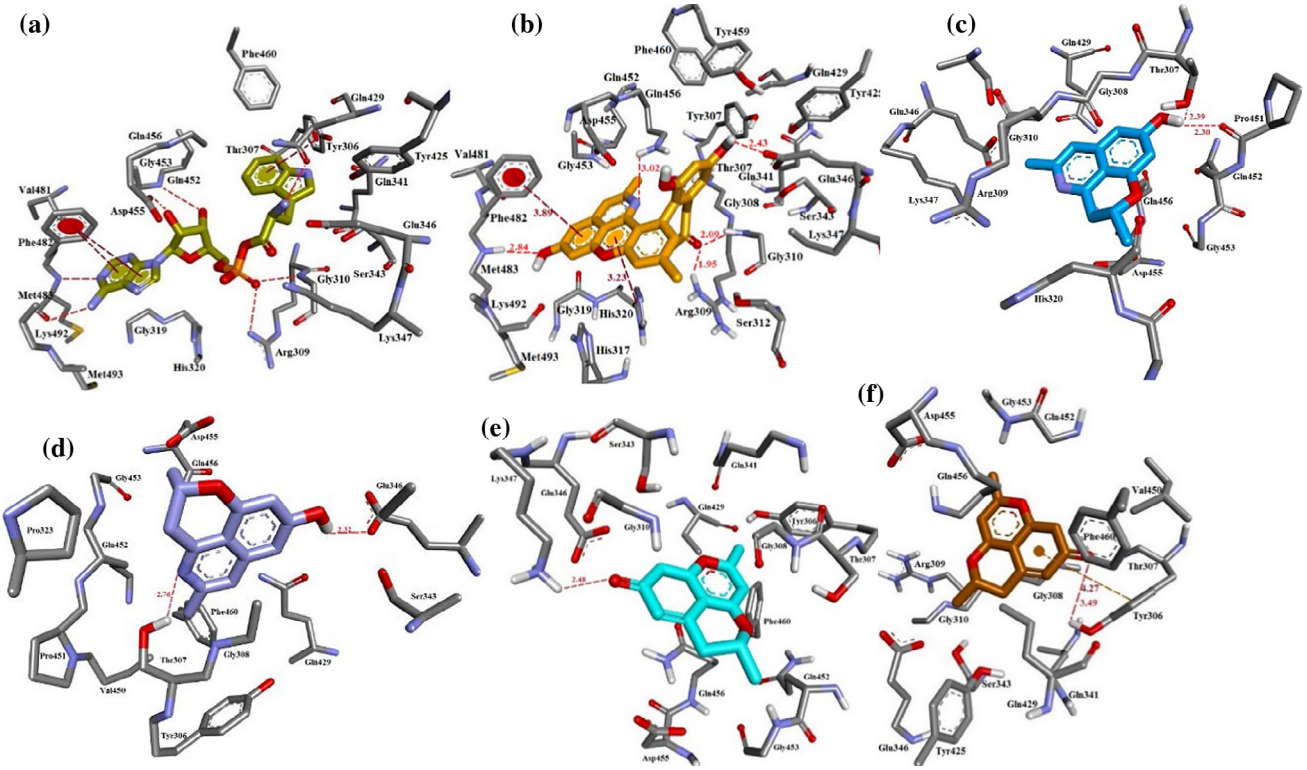

Fig. 2. Illustrating the interaction of the various ligands with tRNA synthetase: (A) Binding of WAMP (B) Binding of Cassiarin F (Orange) (C) Binding of *R*-Cassiarin C (Blue), (D) Binding of *S*-Cassiarin C (Violet), (E) Binding of *R*-DHB (Cyan); (F) Binding of *S*-DHB (Brown).

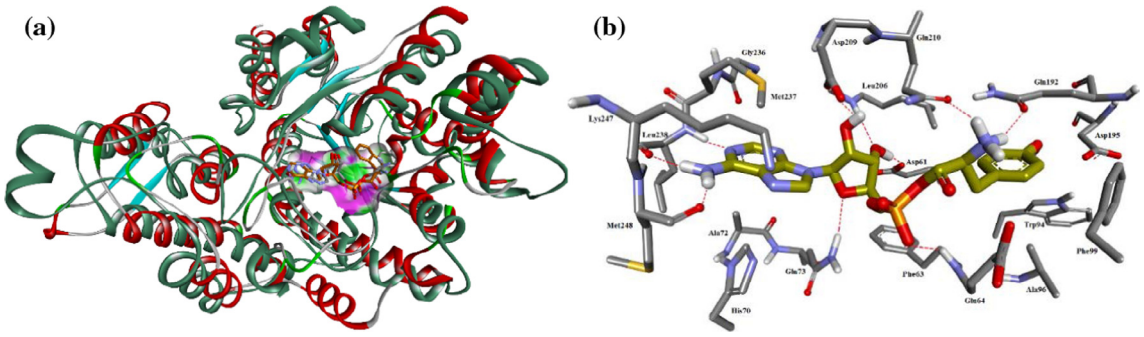

Fig. 3. (A) Superposition of active site domain of Tyrosyl-tRNA synthetase (secondary structure ribbon colour; grey colour code for co-crystallise ligand) and *Pf-c*TrpRNA (secondary structure in green colour; brown colour code for co-crystallise ligand); (B) interactive mode of co-crystallise ligand with Tyrosyl-tRNA synthetase.

pyridine ring of its isoquinoline core binds like adenosine ring of AMP as it utilises His70 (T-shaped π-π interaction, 3.59 Å) and Lys247 (*H*-bond acceptor interaction, 2.67 Å) of KMSKS conserved motif, shown in Fig. 4(B) (Sinnokrot and Sherrill, 2004). Similar to *S*-Cassiarin-C, the binding conformation of *R*-DHB also utilises AMP binding pocket, as: (a) quinone has *H*-bond acceptor interaction with Gly207 backbone (2.03 Å); (b) The 2-methyl-2*H*-pyran ring mimic the adenosine ring binding region through *H*-bond acceptor interaction with the side chain of Lys247(2.02 Å), see in Fig. 4(C).

3.4. 1-Deoxy-D-xylose-5-phosphate reductoisomerase (DXR)

DXR (PDB: 4Y67, *Res.* 1.6 Å, (Chofor et al., 2015)) is a class B dehydrogenase enzyme, which exists as a homodimer in its active form (the active region started from Lys75 to Ser488) where each monomer is made up of two large domains separated by a cleft containing a deep pocket, a linker region, and a small *C*-terminal domain (Chofor et al., 2015). One of the large domain is responsible for NADPH binding (region started from 77 to 230), and the other domain is for catalysis (contains, metal and substrate binding, region started from 231 to 369). The catalytic domain is an α/β-type structure, consisting of five α-helices (α_7–α_{11}) and four β-strands (β_8–β_{11}) and have two different conformations, open and closed. The open conformation assist the substrate *D*-xylose-5-phosphate (DXP) to enter and binds to the active site (Mac Sweeney et al., 2005; Umeda et al., 2011). On the other hand, the NADPH binding site, contain conserved residues (Asp231, Glu233, Ser269, Ser270, Trp296, Met298, Ser306, Asn311, Lys312, and Glu315), which are also conserved in all human malaria parasites (Yajima et al., 2007; Kunfermann et al., 2013).

However, the most studied inhibitor class, fosmidomycin and its analogues bind in a typical fashion to DXR protein (Chofor

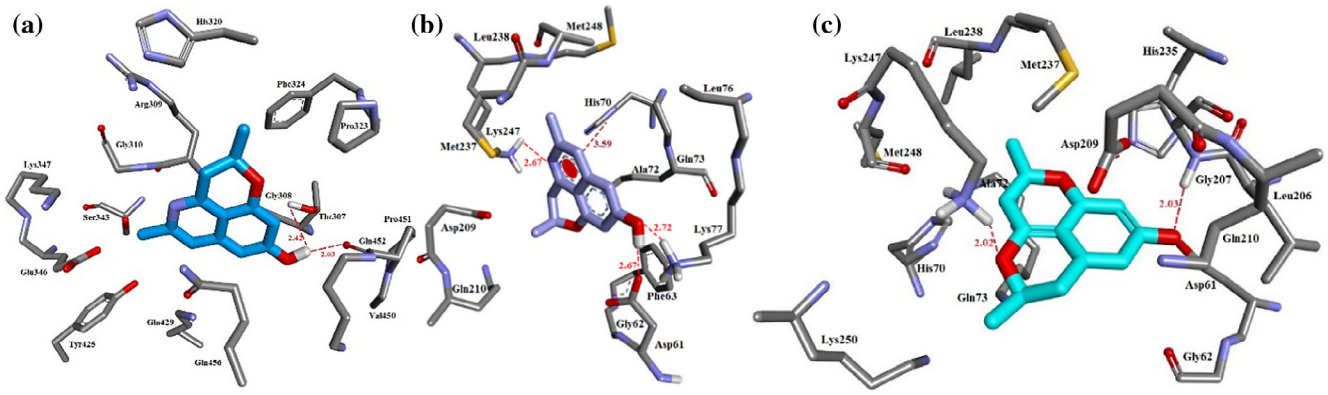

Fig. 4. Molecular binding poses: (A) *R*-isomer of Cassiarins-C (blue) shows its utilises the GIDQ conserved domain (presence of Asp209, Gln210); (B) S-isomer (violet) of Cassiarins-C binds to adenosine monophosphate cavity; (C) *R*-DHB (cyan).

et al., 2015), which can further categorised into three regions (a) phosphate head (PO_4) binding region, which has tight *H*-bond interaction network with Ser270, Asn311, two water molecules, and His293; (b) hydrophobic carbon backbone binding region, which runs parallel to the indole ring of Trp296 and interacts with Met298; (c) hydroxamate binding pocket, which coordinated in *cis*-arrangement with metal ion (Mg^{2+} or Mn^{2+}), negatively charged residues (Asp231, Glu233, and Glu315) and forms a typical distorted trigonal bipyramidal geometry for these class of compounds (Fig. 5(A)).

The molecular docking of Cassiarin-F shows its resorcinol phenolic functionality utilises majorly hydroxamate binding region, as characterised by its *H*-bond interaction with the backbone of Ser269 (3.18 Å), His341 (2.65 Å) and side chain (O*H*) of Ser232 (2.66 Å), as shown in Fig. 5(B). Also, its hydrophobic tetracyclic ring aligns parallel to the Trp296 and Met360, as same like the hydrophobic carbon backbone of the fosmidomycin analogues. Similarly, like Cassiarin-F, the *R*-Cassiarin-C phenol ring fits into the hydroxamate binding region as through the *H*-bond acceptor/-donor interactions with free –NH_2 side chain of Lys205 and –C*O*O*H* functionality of Asp231 respectively. While, the isoquinoline ring of *R*-Cassiarin-C participates in π-π interaction with Trp296 (3.86 Å & 4.45 Å), which shows its ring orientation different from the F-isoform, in Fig. 5(C). This indicates the pivotal role of additional aryl ring system (i.e. the extended propanone-resorcinol structure of Cassiarin-F), is a key difference for the such binding conformation of Cassiarin-F when compared to the binding conformation of *R*-Cassiarin-C.

Structurally, Cassiarin-C and Cassiarin-D are only different at C_2-position substitution with 5-propenone-7-hydroxy-4*H*-chromen-4-one. The molecular docking of *S*-Cassiarin-D shows the 5-propenone functionality imitate like phosphate head and binds to Ser270 (side chain (1.61 Å) and backbone (1.92 Å)), backbone of Gly271 (2.54) and side chain (O*H*) of Ser269 (2.37) *via* H-bond acceptor interactions. While, the non-aromatic quinone interact with NH_2-terminal of Glu233 (2.83 Å) through *H*-bond acceptor interaction. It appears that C_2 extension from Cassiarin-C to Cassiarin-D pushed the tricyclic isoquinoline core more towards the NADPH binding pocket region (as provided with the presence of Ser88 and Ile89 from the of NADPH binding site) and, also aligned with the hydrophobic backbone patch (presence of Trp296 and Met360), shown in Fig. 6(A). However, *H*-bond acceptor interaction of N_1-isoquinoline with N*H*-indole side chain of Trp296 (1.90 Å), shows the tricyclic ring tossed up from the cavity, which could be interesting to observe in case of co-binding of NADPH as its adenine ring would be close within 4.5 Å distance for π-π interaction with isoquinoline ring of *S*-Cassiarin-D. While in case of *R*-DHB, the quinone ring binds to phosphate head region *via H*-bond acceptor interaction with side chain of Ser270 (3.08 Å), backbone of Ser269 (2.03 Å) and NH_2-terminus of side chain of Lys312 (2.34 Å), in Fig. 6(B). Additionally, the incorported *O*xygen atom of 2*H*-dihydropyran core of *R*-DHB shares a *H*-bond acceptor interactions with side chain of Ser232. Also, it has been found interesting that the interactive mode of *R*-DBH couldn't find characteristic hydrophobic backbone binding residues like Trp296 and Met360 within 4.5 Å. However, in case of molecular binding of *S*-DHB, quinone ring interacts (N*H*2 terminal of Lys 205 (2.63 Å) and Asn311 (2.89 Å)), *via H*-bond acceptor interactions, similarly like quinone ring of *R*-isomer, shown in Fig. 6(C) and Fig. 6(B), respectively, but its C_2 associated pyran ring proximity to the

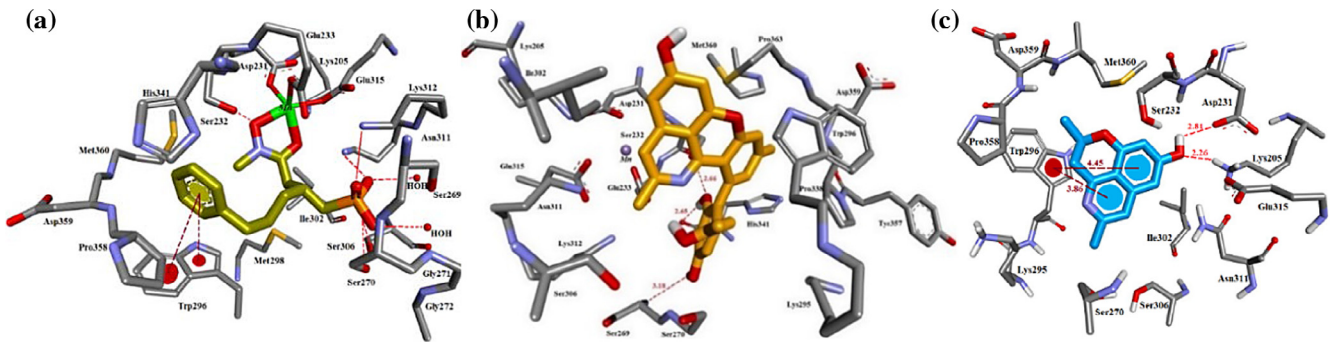

Fig. 5. Interactive binding mode: (A) Co-crystallise fosmidomycin derivative (gold); (B) Cassiarin F (Orange); (C) *R*-Cassiarin-C (Blue).

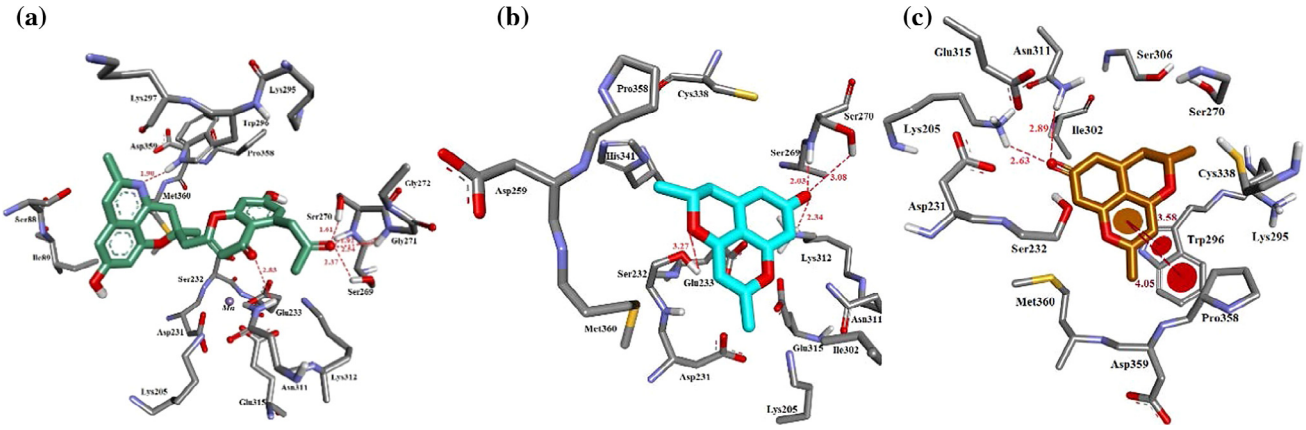

Fig. 6. Binding mode: (A) *S*-Cassiarin-D (green); (B) *R*-DHB (cyan); (C) S-DHB (brown).

Trp296 (hydrophobic interactions, 3.58 Å and 4.05 Å) and Met360, shows the critical role of C_2 stereochemistry in their binding to the DXR protein, as it was not seen in *R*-isomer. We also found these Cassiarins binding lacks the utilisation of hydroxamate cavity of DXR protein and hence unable to coordinate with Mn^{2+} ions and to form typical trigonal bipyramidal geometry, as seen in fosmidomycin class inhibitors.

3.5. Glycerol kinase (*Pf*GK)

*Pf*GK (PDB: 2 W41, *Res.* 2.41 Å, (Schnick et al., 2009)) phosphorylate the glycerol, which is a rate-limiting step in glycerol utilisation in parasite metabolism (Schnick et al., 2009; Naidoo, 2013). Deletion of host gene shows no effect on gametocyte development, suggesting that these life cycle stages do not utilize host-derived glycerol as a carbon source (Schnick et al., 2009). The structural architecture of *Pf*GK contains 501 amino acid residues, arranged in two domains separated by a deep cleft. Each domain is constructed around a α/β core (characterise as $\beta\beta\beta\alpha\beta\alpha\beta\alpha$) that is characteristic of the sugar kinase/Hsp70/actin superfamily proteins (Bork et al., 1992; Hurley, 1996). The Domain I (regions 1–262 and 436–471) comprises $\beta_3\beta_2\beta_1\alpha_1\beta_5\alpha_6\beta_{12}\alpha_9$ and domain II (regions 263–435 and 472–501) consists of $\beta_{16}\beta_{14}\beta_{13}\alpha_{12}\beta_{19}\alpha_{13}\beta_{20}\alpha_{14}$ (Schnick et al., 2009).

However, domain 1 is responsible for glycerol binding and domain II is for ADP binding. The adenine base of ADP slipped into a pocket of domain II and the ribose-phosphate functionality pointed towards the interdomain cleft. The nucleoside (adenine-

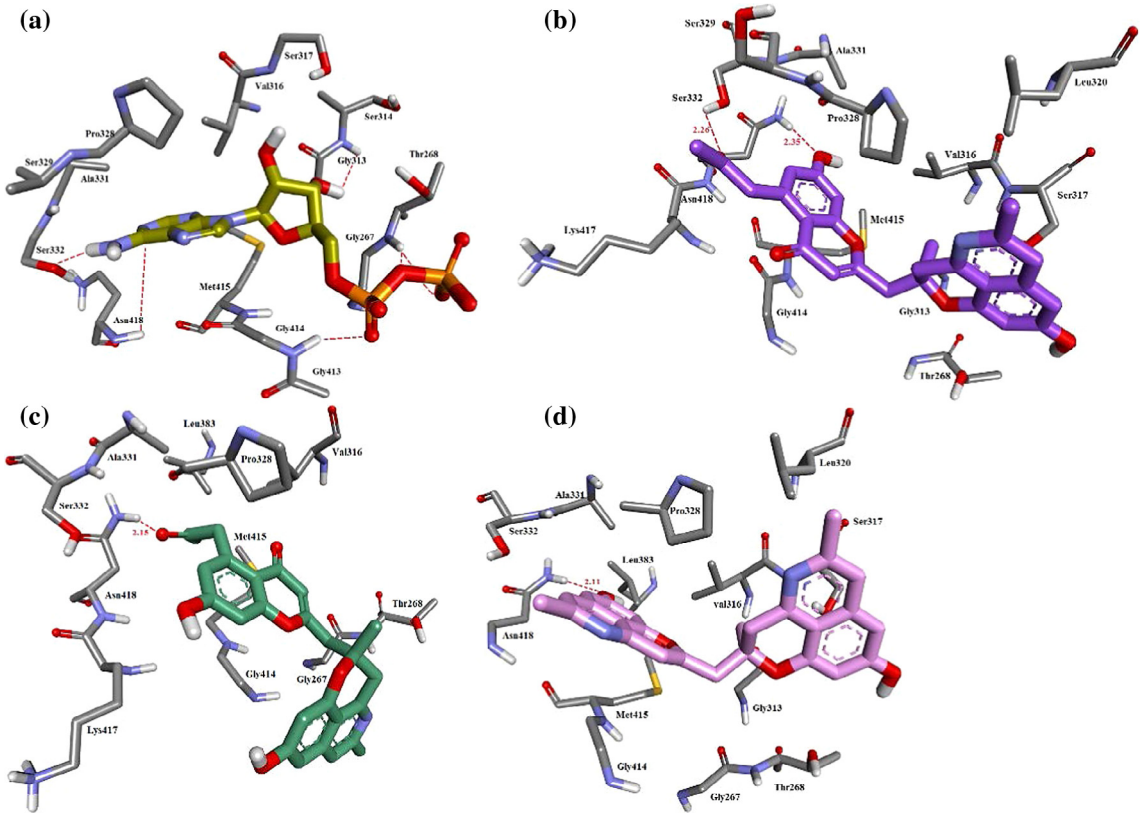

Fig. 7. Interactive mode (A) co-crystallise ADP (gold); (B) *R*-Cassiarin D (purple); (C) *S*-isomer of Cassiarin-D (green); (D) *R*-Cassiarin-E (pink).

sugar) shows typical, kinase domain triad interactions (*H*-bond acceptor/donor/acceptor interactions (Negi et al., 2013b)) with kinase domain (Asn418, Ser332 and Gly313) of *Pf*GK. The phosphate binding pocket surrounded by Gly267, Thr268, Gly413 and Gly414 are profoundly required in the ternary closed complex with ATP. While, sugar binding pocket constituted by residues like Gly313, Ser314 and Met415 (Hurley et al., 1993; Schnick et al., 2009), see in Fig. 7(A).

The phenolic (O*H*) and propanone functionalities of 5-propenone-7-hydroxy-4*H*-chromen-4-one of *R*-Cassiarin-D utilises triad interaction like adenine, with backbone of Asn418 (2.35 Å) and side chain of Ser332 (2.26 Å), as shown in Fig. 7(B). Although, *S*-isomer of Cassiarin-D also interacted with Asn418 (2.15 Å) in a similar fashion like *R*-isomer, but as because C_2 stereochemistry changes in both isomer, the remaining halves of both isomers oriented differently, as *R*-isomer extended towards Leu320, over Thr268 while *S*-isomers twisted in L-shaped into the vicinity of Thr268, shown in Fig. 7(C). However, the presence of Pro328 and Met415 parallel to the C_2 tethered backbone in both stereoisomers binding conformations, showed their utilisation of sugar binding region. Also, *R*-Cassiarin-E follows the same trend as like Cassiarin-D isomers binding with kinase region, as its phenolic O*H* involved in *H*-bond donor interactions with backbone of Asn418 (2.17 Å). However, *R*-Cassiarin-E doesn't have 5-propenone-7-hydroxy-4*H*-chromen-4-one functionality like Cassiarin-D isomers, but has *bis*-tricyclic system, which encloses most of the Cassiarin-D isomers binding cavity residues, Fig. 7(D).

3.6. Plasmodium falciparum Arginase (PfAI)

*Pf*AI (PDB: 3MMR, *Res.* 2.14 Å, (Dowling et al., 2010)) has close resemblance with its human homologous proteins, human arginases I (*Hs*AI, 28%) and II (*Hs*AII, 27%) and also utilises binuclear manganese (Müller et al., 2005). The interactive mode of co-crystallise ligand (2(*S*)-amino-6-boronohexanoic acid, ABH) of the *Pf*AI illustrated the key important residues of the active site, as it has *H*-bond interactions with Glu368, Asp274, Ser229, Asn222 and forms tetrahedral geometry with both the manganese atoms (Wells et al., 2009; Dowling et al., 2010), see in Fig. 8(A).

The molecular docking of these Cassiarins shows their utilisation of the ABH binding cavity. Whereas, the *R*/*S* isomer of Cassiarin-C flipped their orientations, displaying the influence of their C_2 stereochemistry and relatively small molecular size with regards to the cavity size, shown in Fig. 8(B) and (C), respectively. Their flipping in orientation can be further understood based on their interactions as the phenolic (O*H*) and *O*-pyran ring of *R*-Cassiarin-C has *H*-bond acceptor interactions with His218 (2.77 Å) and Thr337 (2.80 Å) while, the phenolic (O*H*) of *S*-Cassiarin-C has *H*-bond donor interactions with Asp274 (2.24 Å) and Glu277 (2.57 Å) and its *O*-pyran ring has *H*-bond acceptor with Asn222 (2.44 Å). On the other side, the *S*-DHB shows *H*-bond acceptor interactions with side chain of Ser229 (2.99 Å) and Asn222 (2.08 Å), as shown in Fig. 8(D). These isoforms binding utilises only one manganese metal ion for coordination in their 4.5 Å, which is irrespective to the conventional inhibitors as their binding utilises two manganese atoms. This point could be useful in developing a hepatic antimalarial drug in future, as *Pf*AI has been critical for malarial parasites during their liver stage development.

3.7. Nucleosome assembly protein

P. falciparum contains two nucleosome assembly proteins termed *Pf*NapL and *Pf*NapS (Chandra et al., 2005). *Pf*NapL (PDB: 3FS3, *Res.* 2.3 Å, (Gill et al., 2009)) is a 347-amino acid dimer, cytoplasmic localised protein and has a central core of ~250 residues that are thought to be responsible for histone binding. *Pf*Nap composed of two domains, domain-I (consists, dimerization helix-2, region started from 37 to 87) and domain-II, containing multiple

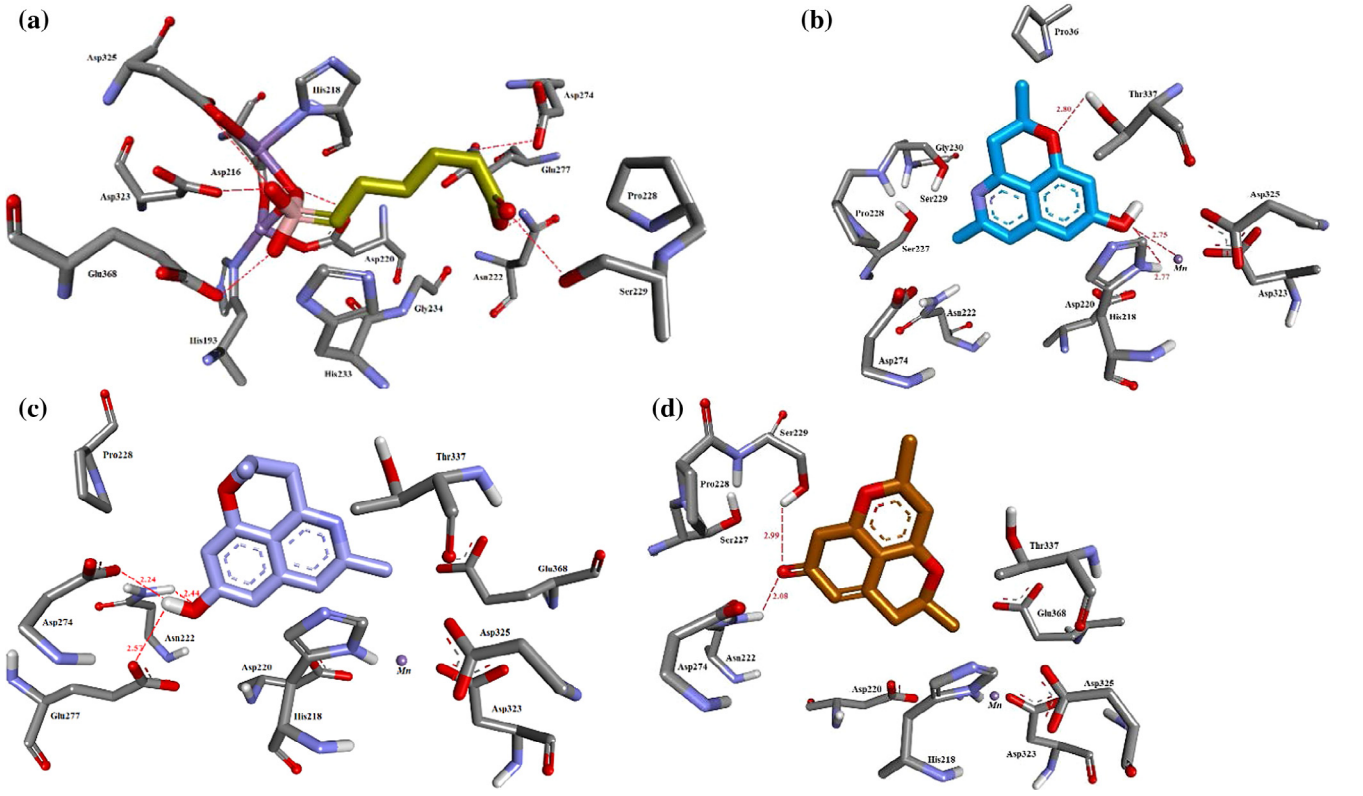

Fig. 8. Interactive binding mode: (A) co-crystallise ABH (gold); (B) R-Cassiarin-C (blue); (C) S-Cassiarin-C (violet); (D) S-DHB (brown).

α-helices and a subdomain containing four antiparallel β-strands (amino acid residues 128–185) (Gill et al., 2009). The dimerization helix-2 of domain-I forms the distinguishing shape of *Pf*NapL, where two backbone helices cluster in an antiparallel manner to form the dimer using mainly hydrophobic interactions and salt bridges or hydrogen bonds (Gill et al., 2009).

The *R*-Cassiarin-E binds in a V-shaped, as shown in Fig. 9(A), where both aromatic cores go inside to the cavity composed of α_2 (Arg68, His72 and Tyr 75) of dimerization helix-2, α7 (Tyr272, Pro271, Lys266 are the residues involved), Gly145 and Phe146 at the tip of β_2, and Met169, Val179 are in the loop in between β_3 and β_4, and exposes its CH_2-tethered backbone to the surface, as seen in Fig. 9(A). Whereas, its *O*-dihyropyran ring and phenolic *O*H interacts with NH_2 terminus of Lys266 (3.20 Å) and N*H*-imidazole side chain of His72 (2.28 Å), respectively. While, in case of *S*-DHB, the pyran ring faces towards Cys133, Tyr79, encloses into a cavity composed of Lys266, Glu267, Ile270 and Pro271 on one side and Arg68, His72 and Tyr135 from other side (see, in Fig. 9(B)).

3.8. Adenylosuccinate synthetase (PfAdSS)

Each subunit of *Pf*AdSS (PDB: 1P9B, *Res*. 2.0 Å (Eaazhisai et al., 2004)) consists of 19 strands (β_1-β_{19}), 12 α-helices, seven 3_{10} helices and 6 loops ($L_{1\text{-}5}$). Nine parallel β-strands (β_9, β_7, β_5, β_2, β_{10}, β_1, β_{11}, β_{15} and β_{18}) along with a tenth antiparallel strand (β_{19}) forms a central sheet. This sheet is bordered by four subdomains: (a) subdomain-I (residues 54–65) comprises of only two β-strands (β_3 and β_4); (b) subdomain-II (residues 114–206) mainly involved in interface interactions; (c) subdomains-III (residues 278–302) majorly constitute ligand binding pocket; (d) subdomain-IV (residues 339–418). It has 2 binding sites: orthosteric (IMP binding site) and allosteric (GTP binding site). Both sites are close to each other. The previous studies highlighted various structural features and key residues of active site, as summarised here, (Eaazhisai et al., 2004): (a) Lys31 (which is a conserved residue in active site); (b) Lys62 (forms *H*-bonds with ribose hydroxyls in *Pf*AdSS but absent in the other homologous AdSS proteins); (c) Lys29 is highly involved in phosphate head binding of GDP and shares a typical *H*-Bond character (Low Barrier Hydrogen Bond, LBHB, (Cleland and Kreevoy, 1994)); (d) phosphate binding pocket majorly constituted by the residues, like Asp26, Lys29, Gly53, His54 and Asn232; (e) Asp26 is believed to be a key residue which gets protonated and later coordinated to Mg^{2+} (Choe et al., 1999; Iancu et al., 2002). (f) Asn232, which interacts with IMP, similarly present in the *E. coli* and mouse AdSS complexes, (g) LBHB interaction of His54 and O_2 of 6-phosphoryl of IMP (2.54 Å), is parallel to the mouse synthetase complex (2.46 Å) (Cleland and Kreevoy, 1994; Iancu et al., 2002).

The molecular docking of *R*-DHB shows, its pyran ring utilise the N*H*-guanidine side chain of Arg313 of β_{13} (2.16 Å & 2.30 Å) and alcoholic (O*H*) side chain of Thr307 of most conserved segment of loop L_5 (2.62 Å) *via* H-bond acceptor interactions, see in Fig. 10 (A). However, its binding pocket shows conserved helix α_1($G^{28}L^{29}$-$G^{30}K^{31}$), L_5 region containing {($H^{303}Y^{305}T^{307}$), β_{13} (R^{313}) and L_6 (P^{428}) of the *Pf*AdSS. However, *S*-DHB also shows similar binding like R-DHB to the pocket, like α_1($L^{29}G^{30}K^{31}$), β_3 (H^{54}), L_5 ($E^{304}T^{307}$), β_{13}(R^{313}). While, its quinone ring and 2*H*-pyran ring has *H*-bond acceptor interaction with N*H* of backbone of Gly30 (2.15 Å) and N*H* side chain terminus of Lys339 (2.44 Å), as seen in Fig. 10(B).

3.9. Glucose-6-Phosphate isomerase (PfG6PI)

As no further structural information for *Pf*G6PI protein (PDB: 3PR3, *Res*. 2.45 Å, (Gileadi et al., 2011)) was available, hence we evaluated its own co-crystallise ligand (fructose-6-phosphate) binding, to allocate the key residues in its active site. The binding shows its phosphate head has *H*-bond network with Ser159, Ser231, Lys232, Thr233 and Thr236, while polar heads of fructose sugar has *H*-bond interaction with Gly158, Glu380 and Lys540, see in Fig. 11(A). Furthermore, compared with human protein (*Hs*G6PI, PDB:1JLH, *Res*. 2.1 Å (Cordeiro et al., 2003)), *Pf*-G6PI found to have two globular domains (as one, large and other, small domains) and an "arm-like" *C*-terminal tail, similar like *Hs*G6PI of humans. Both the large and the small domain have a central core of a β-pleated sheet flanked by α-helices to form a typical α/β folding motif. The large domain contains 6 β-strands (β_1:^{40}I to ^{42}K; β_2: ^{46}F to ^{52}R; β_7:^{357}N to ^{362}P; β_8:^{400}V to ^{402}F; β_9:^{425}V to ^{430}F; β_{10}: ^{495}S to ^{500}F) and small domain has 4 β-strands (β_3: ^{150}N to ^{154}I, β_4: ^{201}N to ^{205}L; β_5: ^{225}T to ^{230}I; β_6: ^{264}M to ^{267}V).

The molecular docking of *R*-DHB shows its binding complimentary to the fructose-6-phosphate as the presence of residue 156–159 and 231–239 shows the phosphate binding pocket of fructose-6-phosphate, which is situated in between $\beta_{3/4}$ and $\beta_{5/6}$, respectively, as shown in Fig. 11(B). While, *R*-Cassiarin-D shows similar binding orientation to the cavity, situated in $\beta_{5/6}$: Lys232, Thr233, Thr236, flanked α-helix (Gly293, Arg294), $\beta_{7/8}$ (Gln376, Glu380), *C*-terminal tail (Lys540) and enclosed within *H*-bond distance with charged side chains of Glu380 (2.09 Å), Arg294 (2.33 Å) and backbone of Gly293 (2.92 Å), shown in Fig. 11(C).

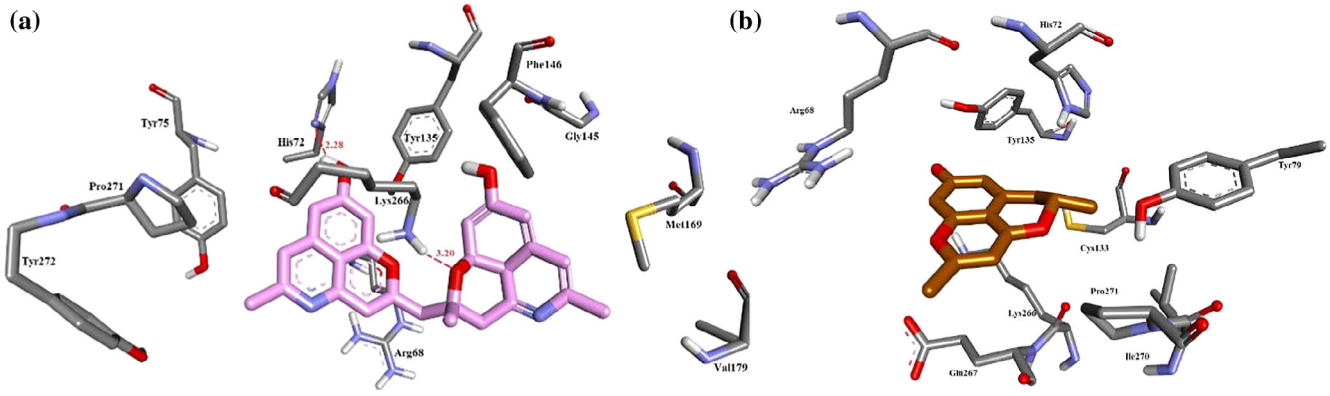

Fig. 9. Interactive binding mode: (A) *R*-Cassiarin-E (pink); (B) *S*-DHB (brown).

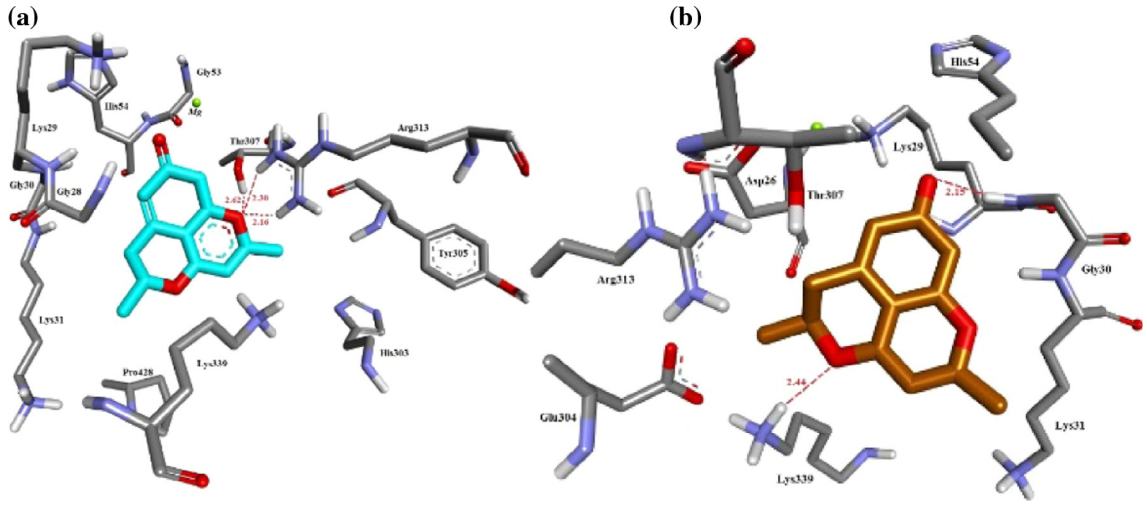

Fig. 10. Interactive mode: (A) R-DHB (cyan); (B) S-DHB (brown).

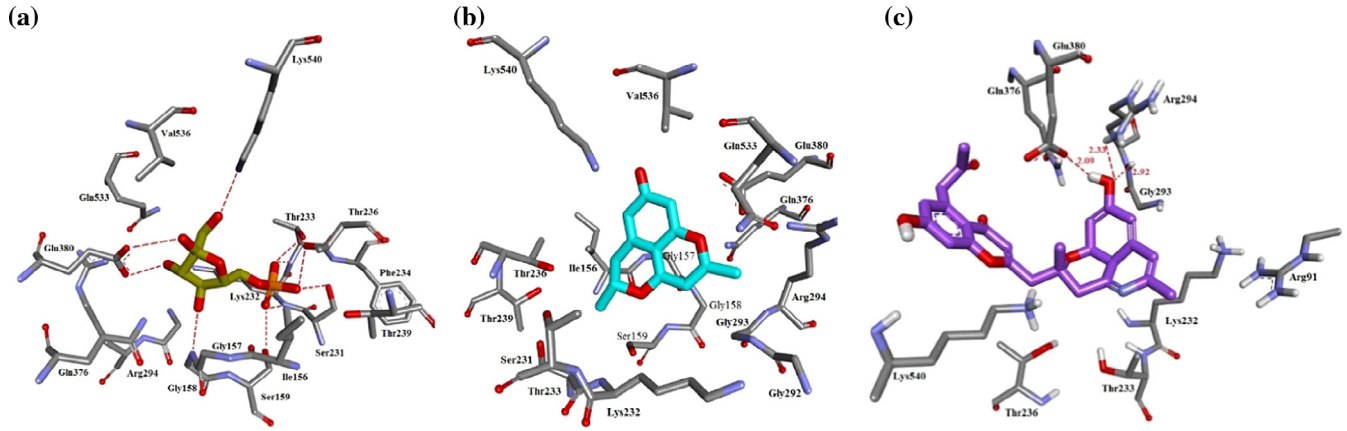

Fig. 11. (A) co-crystallise fructose-6-phoaphate (gold); (B) *R*-DHB (cyan); (C) *R*-Cassiarin-D (purple).

3.10. Kelch motif associated protein of Plasmodium falciparum (PfKEAP)

It is BTB domain containing 389 residues long dimer (PDB: 4YY8, *Res.* 1.81 Å, (Jiang et al., 2015), constituted by 28 β-strands where β_4 to β_{28} involved in the formation of its 6 kelch motifs: Every motif contains 4 β-strands in common, except motif 5, which has unusual 6 β strands (***K*****$_1$**: $\beta_4^{\text{L444-I448}}$, $\beta_5^{460\text{-}464}$, $\beta_6^{469\text{-}472}$, $\beta_{29}^{\text{Ser720-Ala724}}$; ***K*****$_2$** $\beta_7^{484\text{-}489}$, $\beta_8^{491\text{-}495}$, $\beta_9^{508\text{-}512}$, $\beta_{10}^{517\text{-}520}$; ***K*****$_3$** $\beta_{11}^{532\text{-}536}$, $\beta_{12}^{539\text{-}543}$, $\beta_{13}^{555\text{-}559}$, $\beta_{14}^{564\text{-}567}$; ***K*****$_4$** $\beta_{15}^{579\text{-}583}$, $\beta_{16}^{586\text{-}590}$, $\beta_{17}^{601\text{-}605}$, $\beta_{18}^{610\text{-}613}$; ***K*****$_5$** $\beta_{19}^{622\text{-}624}$ $\beta_{20}^{627\text{-}630}$, $\beta_{21}^{633\text{-}637}$, $\beta_{22}^{640\text{-}642}$, $\beta_{23}^{650\text{-}654}$, $\beta_{24}^{659\text{-}663}$; ***K*****$_6$** $\beta_{25}^{674\text{-}678}$, $\beta_{26}^{682\text{-}685}$, $\beta_{27}^{696\text{-}700}$, $\beta_{28}^{705\text{-}709}$). These 6 kelch motifs together built a propeller architecture, shown in Fig. 12(B). Further comparative sequence and structure studies with human (*Hs*KEAP, PDB: 4XMB, Res. 2.43 Å) (Jain et al., 2015) and mouse (*Mm*KEAP, PDB: 4ZY3, Res. 1.80 Å) (Saito et al., 2016) kelch motif containing proteins, show key residues associated with the orthosteric binding site, Fig. 12(A).

The co-crystallise ligand (mono-alkylated *p*-substituted sulphonamides) of *Hs*KEAP1 fits in between cavity surrounded by kelch repeats $K_{3/4/5}$: $F^{451}Y^{456}Y^{482}N^{498}R^{529}$ $N^{530}Y^{546}I^{551}S^{576}S^{577}T^{593}G^{595}$-$E^{596}R^{597}S^{623}S^{624}$ of *Pf*KEAP, shown in Fig. 12(C). The cross docking of co-crystallise ligand of *hs*KEAP1 on *Pf*KEAP, shows distinctive kelch motif features in *Pf*KEAP as compare to the kelch motifs of human proteins, as further supported by minimum RMSD value (4.84 Å) and free energy (−7.86) for *Pf*KEAP than minimum RMSD (1.07 Å) and free energy (−7.34) for *Hs*KEAP. While in our observation, we found *R*-Cassiarin-E (−15.2877) and *S*-Cassiarin-C (−12.22) are more profoundly forming energy-stable complexes with *Pf*KEAP. Also, their interactive mode has similar binding pattern as –OH groups of *R*-Cassiarin-E interacts with the backbone of ***K*****$_2$** region through *H*-bond acceptor-donor interactions, as shown in Fig. 13(A). While, the other half, fits in the hydrophobic cavity constituted by aromatic amino acids. On the other side, the *S*-Cassiarin-C uses multi kelch motifs as compared to *R*-Cassiarin-E (***K*****$_2$** (β_7), ***K*****$_4$**(β_{15}), ***K*****$_5$** (β_{19} β_{20}), ***K*****$_6$**(β_{25}), ***K*****$_1$**(β_{29})), for its binding to *Pf*KEAP *via H*-bond acceptor/donor interaction with Ser720 (2.67 Å) and Phe674 (2.41 Å) respectively, as shown in Fig. 13(B).

3.11. Ornithine δ-aminotransferase of Plasmodium falciparum (PfOAT)

*Pf*OAT (PDB:3LG0, *Res.* 2.3 Å, (Jortzik et al., 2010)) is active as a homodimer. Based on the comparative sequence alignment with other OATS (Human: *Hs*OAT, PDB: 2OAT, *Res.* 1.95 Å (Storici et al., 1999); Toxoplasma: *Ts*OAT, PDB: 5E3K, *Res.* 1.73 Å (Filippova et al., 2016)) (shown in Fig. 14(A)), we observed high percentage of conserved residues in the active cavity, which is close to the interface of two subunits. Each subunit contains a pyridoxal-

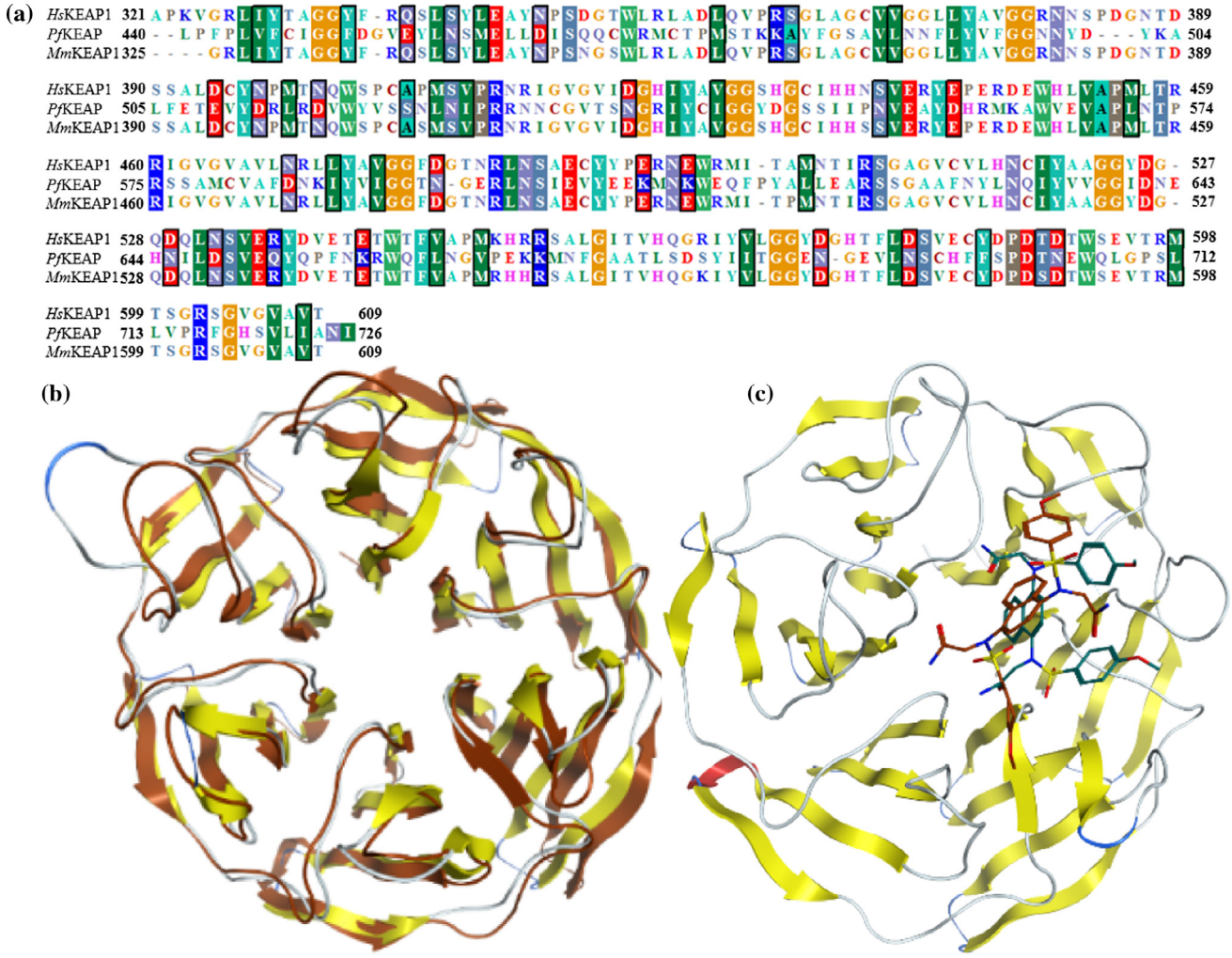

Fig. 12. (A) Multiple sequence alignment (MSA) with human (*Hs*KEAP1) and mouse (*Mm*KEAP1) kelch proteins; (B) Superpose of human (yellow) and *P. falciparum* (brown) kelch protein; (C) Human kelch protein co-crystallise ligand (brown) utilising the similar cavity of *P. falciparum* kelch protein (yellow).

phosphate (PLP) binding domain and a substrate binding domain (Jortzik et al., 2010). The PLP binding loop domain (region started from 287 to 293) is strictly conserved in all species. The *S*-Cassiarin-E binds significantly with the PLP-binding loop domain *via H*-bond donor interaction with amide backbone of Pro286 (2.13 Å) and His289 (2.23 Å); π stacking interaction with imidazole ring of His289 (4.24 Å). Furthermore, N_1-isoquinoline (2*H*) has *H*-bond acceptor interaction with N*H*-guanidine side chain of Arg83 (2.10 Å). While the 2*H*-isoquinoline ring folded towards a hydrophobic cavity (comprises $V^{106}L^{107}M^{108}M^{109}$) which allows the Cassiarin-E to undergo the specific binding conformation, shown in Fig. 14(B).

3.12. Enoyl acyl carrier protein reductase (PfENR)

Previous studies on the protein, enoyl acyl carrier protein reductase obtained from different origins (*P. falciparum*, *E. coli*, *B. napus*, *M. tuberculosis*, *H. pylori*) show overall identical structural homology (Pidugu et al., 2004). This analysis also provides the key features, related to the substrate binding loop region, which were further correlated with the affinities of its conventional inhibitor class, Triclosan derivatives (Belluti et al., 2013). The Triclosan derivatives are primarily contain the Biphenyl ether scaffold (Ring A and Ring B separated by an oxygen atom). In case of *Pf*ENR, the binding of Triclosan (PDB: 3LT0, *Res.* 1.96 Å, (Maity et al., 2010)) typically forms a ternary complex as *Pf*ENR-NAD^+-Triclosan, where ring A of Triclosan settles into a hydrophobic pocket (composed of Tyr277, Tyr267, Gly313, Pro314, Ile323, Phe368, Ile369, and Ala372) and has π-stacking interaction distance with nicotinamide ring of the cofactor NAD^+ (Maity et al., 2010), in Fig. 15(A). While, Ring B of triclosan has close proximity with ribose-phosphate functionalities of NAD^+, substrate-binding loop residues (like Ala319, Ala320, and Ile323) and a conserved loop (containing Ala217, Asn218, Ala219, and Val222) (Pidugu et al., 2004).

The molecular modelling of Cassiarin-E advocates the binding to the co-factor binding site irrespective to the expected substrate binding site. The tricyclic ring of *R*-Cassiarin-E forms the sandwich-type π-π interactions with indoyl moiety of Trp131 (3.82 Å, 4.08 Å, 4.58 Å, 3.73 Å, 3.89 Å & 4.29 Å). While, the remaining part of the molecule twisted towards the ribose-phosphate sugar pocket of NADH, which was also a binding pocket of Ring B of Triclosan, see in Fig. 15(A). This tricyclic ring of this twisted half also has *H*-bond donor/acceptor interaction with Asp107 (2.34 Å) and N*H* backbone of Ala217 (2.90 Å) of cavity domains (comprising $G^{106}D^{107}N^{109}G^{110}$ and $S^{317}R^{318}A^{319}$) on one side and $A^{217}N^{218}$ on other side, respectively, as shown in Fig. 15(B).

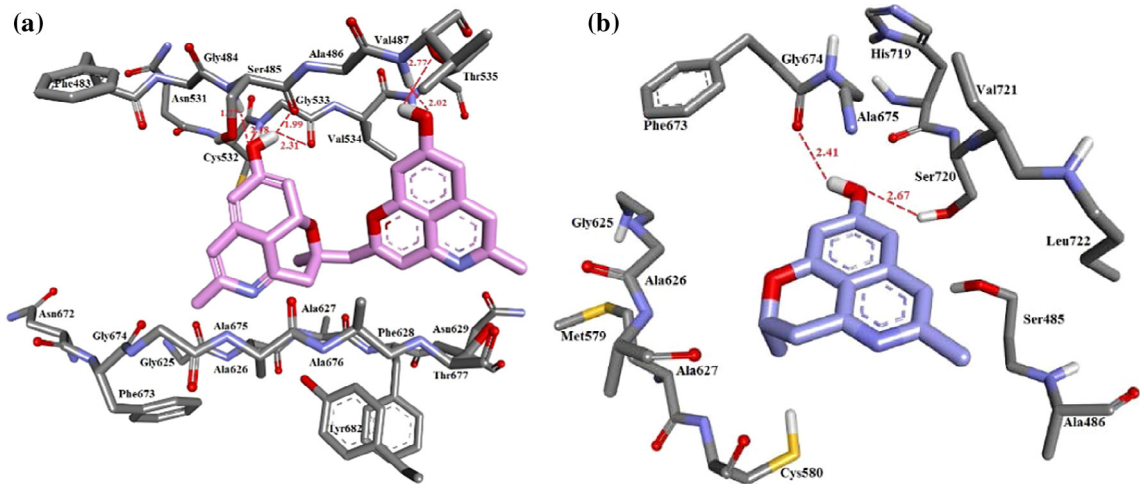

Fig. 13. (A) MSA of *Pf*OAT with *Ts*OAT and *Hs*OAT. (B) Interactive domain of *S*-Cassiarin-E (yellow).

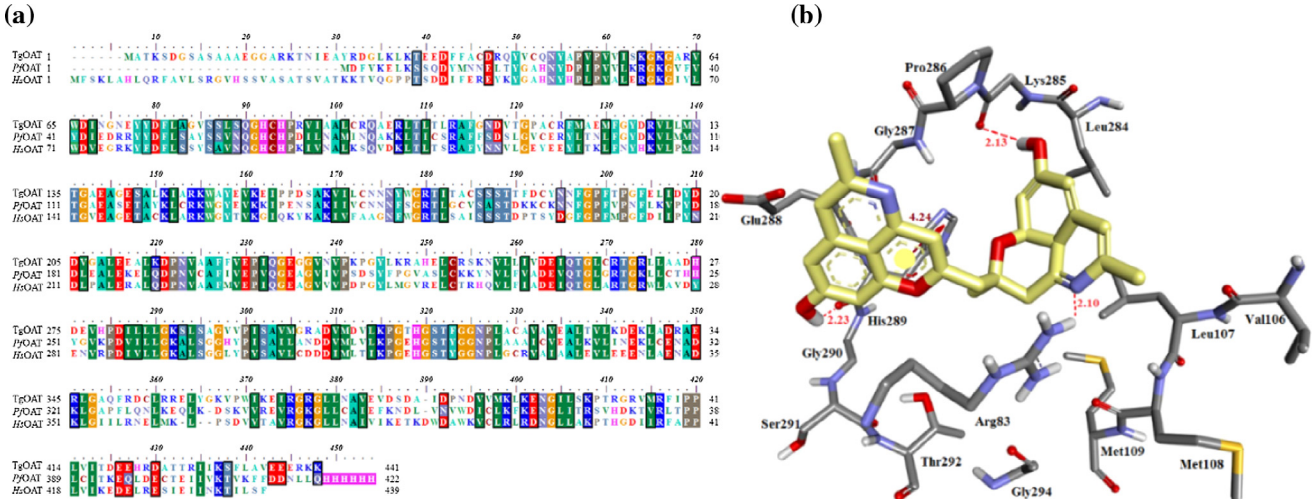

Fig. 14. Interactive binding mode: (A) *R*-Cassiarin-E (pink); (B) *S*-Cassiarin-C (violet).

3.13. Oxoacyl acyl-carrier-protein reductase (FabG)

Most of the interactive domain information for 3-oxoacyl acyl-carrier-protein reductase (PDB:2C07, *Res.* 1.50 Å, (Wickramasinghe et al., 2006)) was limited to Triclosan orthosteric site inhibition, while co-factor binding was highly underestimated. Therefore, we explore the co-factor binding site (NADPH binding site) with 3-oxoacyl acyl-carrier-protein reductase of *E. coli* (PDB: 1Q7B, *Res.* 2.05 Å, (Price et al., 2004)), found RMSD of their backbone (1.455 Å, for 237 amino acids), identity (47.1%) and similarity (68.0%) and with 4 key mutations, as indicated, in Fig. 16(A): Ser99 (Gly41 in *E. coli*), Ser94 (Ala36 in *E. coli*), Arg95 (Thr37 in *E. coli*) and Ser198 (Gly137 in *E. coli*). The molecular modelling studies revealed the binding of *R*-isomer of Cassiarin-E, majorly utilises the binding cavity of nicotinamide functionality of NADP, in Fig. 16(B). However, its *H*-bond donor/acceptor interaction with backbone (–N*H*) of Ser98 (2.68 Å) and phenolic (O*H*) of Tyr212 (2.01 Å) side chain, evident its binding to the phosphate binding cavity of NADP. The tricyclic aromatic ring of R-Cassiarin-E has T-shaped π-π interaction of Phe244 (3.55 Å & 3.79 Å) (Sinnokrot and Sherrill, 2004), as shown in Fig. 16(B).

3.14. Armadillo repeats only protein of Plasmodium falciparum (PfARO)

*Pf*ARO is poor studied protein (PDB: 5EWP, *Res.*1.8 Å (Peifer et al., 1994; Brown et al., 2016)), therefore we compare its structure with the truncated structure of cell adhesion protein of *Caenorhabditis elegans* (PDB:4R11, *Res.* 2.79 Å) (Choi et al., 2015), see in Fig. 17(A). Our investigation found PfARO is 252 amino acid residues long, right handed super helix dimer of 15 α-helixes, which forms a characteristic alpha solenoid structure (Peifer et al., 1994). However, each Armadillo repeat is composed of a pair of alpha helices that form a hairpin structure (involving alpha-helixes: $\alpha_1^{37\text{-}48}$, $\alpha_2^{51\text{-}57}$, $\alpha_3^{81\text{-}93}$, $\alpha_4^{100\text{-}107}$, $\alpha_5^{110\text{-}118}$, $\alpha_6^{123\text{-}136}$, $\alpha_7^{141\text{-}149}$, $\alpha_8^{153\text{-}159}$, $\alpha_9^{165\text{-}179}$, $\alpha_{10}^{183\text{-}191}$, $\alpha_{11}^{194\text{-}200}$, $\alpha_{12}^{215\text{-}228}$, $\alpha_{13}^{236\text{-}243}$, $\alpha_{14}^{247\text{-}254}$, $\alpha_{15}^{260\text{-}273}$; β-strands: $\beta_1^{229\text{-}230}$ and $\beta_2^{233\text{-}234}$). The molecular docking of *S*-Cassiarin-D isomer shows its binding

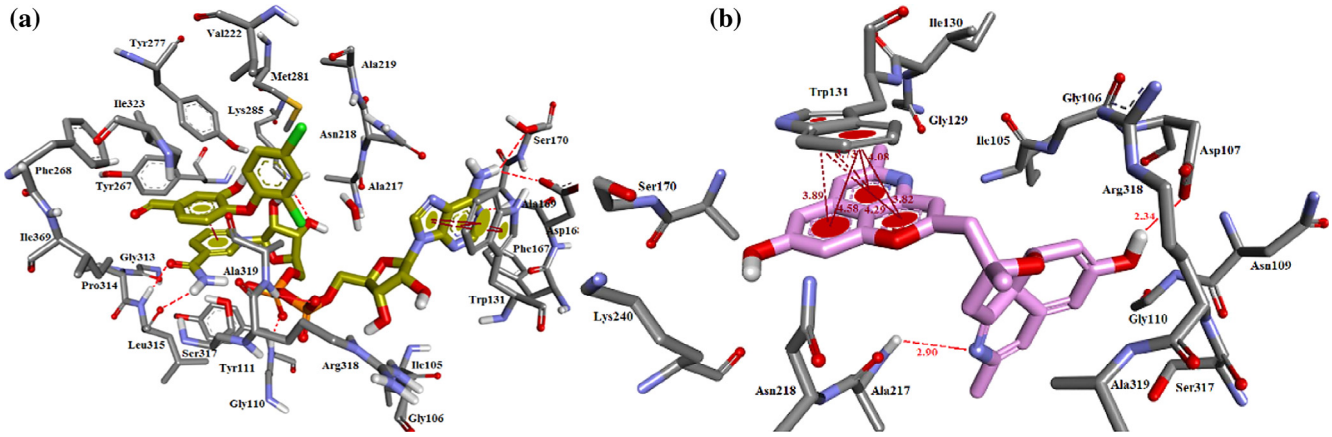

Fig. 15. Interactive binding mode (A) co-crystallise ligand (gold); (B) *R*-Cassiarin-E (pink).

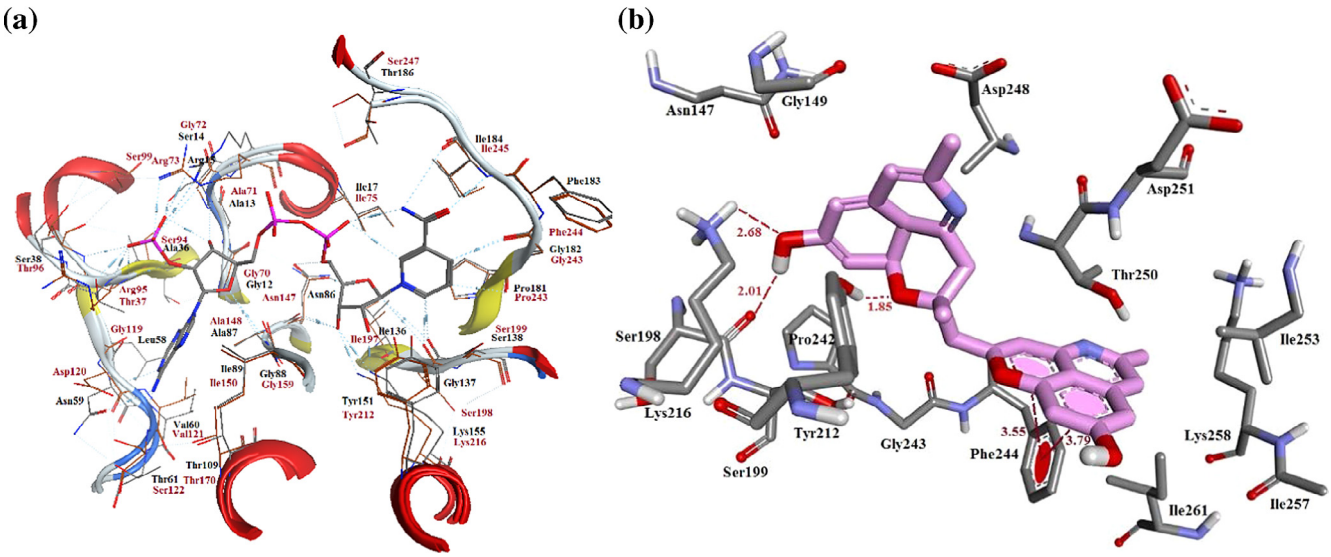

Fig. 16. (A) Superpose of FabG protein of *P. falciparum* (residues labelled in brown) with *E. coli* utilising identical ligand (triclosan derivative) binding orthosteric site; (B) Interactive mode of *R*-isomer of Cassiarin-E.

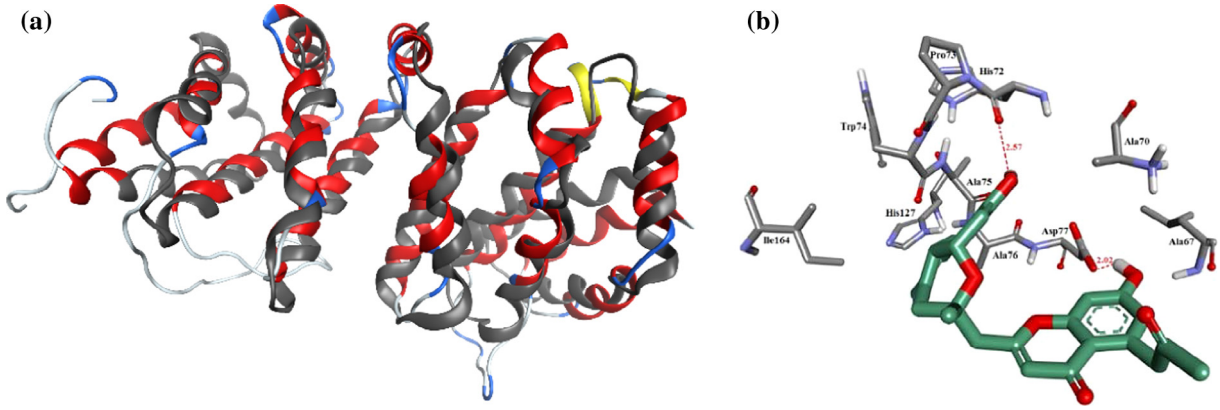

Fig. 17. (A) Superpose with cell adhesion protein of *Caenorhabditis elegans* (grey colour backbone); (B) Interactive mode of *S*-Cassiarin D (green).

dependent on the turn, as enclosed by the interface of $\alpha_{2/3}$ region (containing $A^{67}A^{70}H^{72}P^{73}W^{74}A^{75}A^{76}D^{77}$). Also, its O*H* group shows *H*-bond donor interaction with His72 (2.57 Å) and Asp77 (2.02 Å) with the mentioned interface of $\alpha_{2/3}$ region, in Fig. 17(B).

3.15. Methionine aminopeptidase 1b (*pf*MetAP)

As no structural information related to the *pf*MetAP (PDB: 3S6B, *Res.* 1.95 Å, (Wernimont et al., 2011a,b)) was disclosed by the previous studies, therefore we performed comparative studies of its structure with its human homologous protein (*Hs*MetAP, PDB: 2G6P, *Res*. 1.9 Å, human methionine aminopeptidase Type 1) (Hu et al., 2006). The superimposition of *pf*MetAP and *Hs*MetAP shows the coverage of 81%, RMSD of their backbone (1.253 Å, for 301 amino acids) and identity (54%), as structures shown in Fig. 18 (A). Although, the binding of co-crystallise ligand with *pf*MetAP, shows high resemblance in their orthosteric site, with subtle mutation that could be exploited for selective drug designing and targeting against *P. falciparum* in future, as follow: Thr156 and Ser268 mutated in place of Pro192 and Cys301 (in human), respectively provide *H*-bond donor/acceptor interaction, see in Fig. 18(A). However, the tricyclic ring of *R*-DHB binds in the hydrophobic core (containing $T^{156}Y^{159}F^{162}C^{167}H^{176}$ & $H^{270}F^{276}H^{277}$ W^{320}) and its quinone functionality secured the polar interface of *pf*MetAP constituted by $D^{193}D^{204}E^{303}E^{334}$ (see in Fig. 18(B)).

3.16. Guanosine monophosphate synthetase (GMP synthetase)

GMP synthetase (PDB: 3UOW, *Res.* 2.72 Å, (Wernimont et al., 2011a,b)) is dimeric in nature. Each monomer is composed of two catalytic domains, an *N*-terminal independent GATase (1–236) and a *C*-terminal ATPPase domain (237–555) (Ballut et al., 2015). Its dimer form is highly required for its activity as the interface has 108*C*-terminal residues of the ATPPase domain. In this interface,

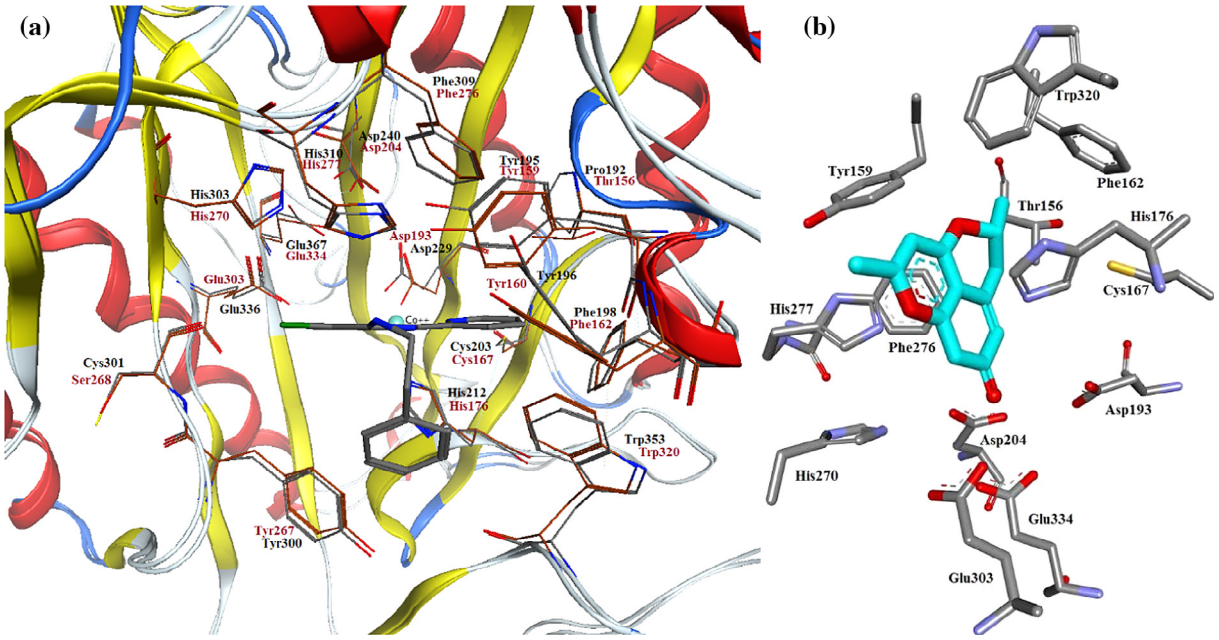

Fig. 18. (A) Comparison of orthosteric site of *pf*MetAP (residues with brown backbone) and *Hs*MetAP (residues with grey backbone) show complimentary evolutionary mutations at Thr156, Ser268; (B) Binding mode of *R*-DHB with *pf*MetAP: utilises the major residues and shows tricyclic core spatially coplanar oriented over Phe276.

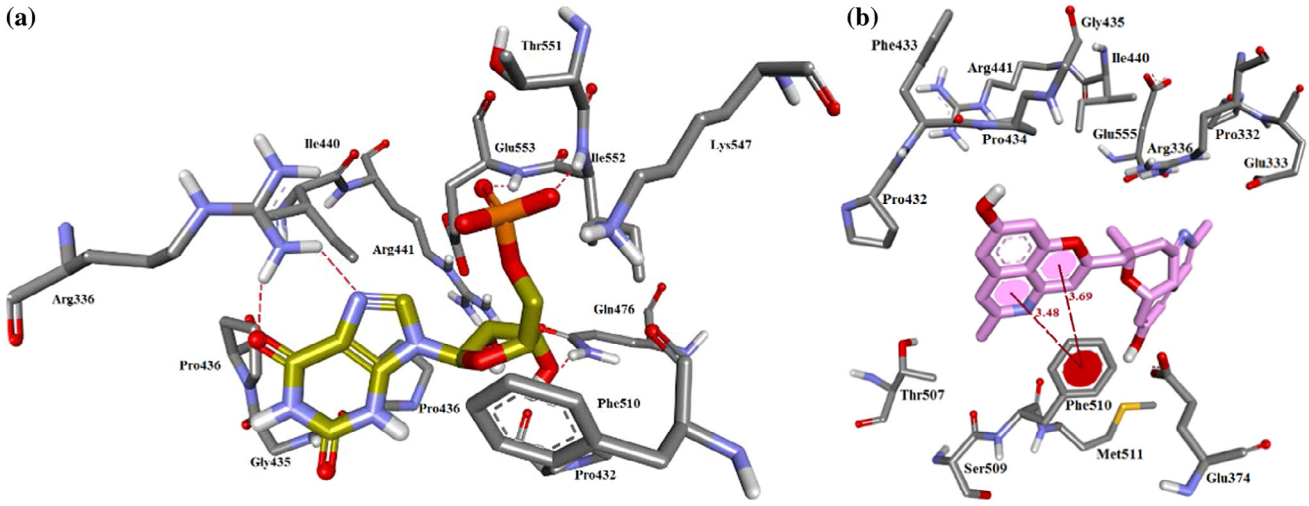

Fig. 19. Interactive binding mode (A) XMP (gold); (B) *R*-Cassiarin-E (pink), with guanosine monophosphate synthetase.

two *cis*-prolines (Pro548–Pro549) allow a tetrahedral configuration of Asp543, Thr551, Glu553 and Arg539 (Ballut et al., 2015). The binding of co-crystallise xanthose monophosphate (XMP) (Gileadi et al., 2011) shows the key residues of ligand binding site of *GMP synthetase*, shown in Fig. 19(A): (a) Arg336, Pro436, Gly435, Pro436 covering the purine face of XMP; (b) the steric hindrance of bulky hydrophobic residues Phe510, Pro432 twisted the ribose sugar towards the polarised domain (constituted by Arg441, Gln476); (c) phosphate heads enclosed by the Lys547, Glu553, Thr551 and Ile552. However, binding of tricyclic ring of *R*-Cassiarin-E fitted to the purine-ribose sugar binding cavity (π-π interactions, 3.69 Å & 3.48 Å with Phe510) while the methylene (–CH_2–) tethered substructure of the molecule (Dihydro-isoquinoline) popped out from the XMP binding cavity, see in Fig. 19(B).

3.17. Merozoite surface proteins duffy binding like Domain-2 (PfMSPDBL2)

The merozoite surface proteins of *P. falciparum* has duffy binding like domains (*Pf*MSPDBL1 and *Pf*MSPDBL2), which helps the merozoite for their initial binding to the surface receptors on the host red blood cell (Wickramarachchi et al., 2009). The duffy binding like (DBL) fold (PfMSPDBL2; PDB: 3VUU, *Res.* 2.09 Å, (Hodder et al., 2012)) consists of residues from 161 to 457 residues, which has a boomerang shaped α-helical core (9 α-helixes) formed from three subdomains (Hodder et al., 2012): (a) subdomain-1 (region 161–225) has only contain 5 residue long α-helix (α_1) and provide a stable junction for subdomain-2 and subdomain-3 by a *H*-bond network (involving Arg-207 (from subdomain 1), Asp-266 (from subdomain-2), and Glu-352 (subdomain-3)); (b) Subdomain-2 (residues 226–341) composed of four structurally conserved helices (helices 2–5); (c) subdomain-3 (344–460) is a helical bundle composed of two long α-helices (α_6 and α_7) and two smaller α-helices (α_8 and α_9) (Hodder et al., 2012). Moreover, a disulfide linkage between Cys441 and Cys444 brings helices α_8 and α_9 are near each other in an anti-parallel manner. The *R*-Cassiarin-D molecular binding mode clearly shows no involvement with subdomain-1 and binds inside the cavity formed by subdomain-2 and subdomain-3: $N^{252}E^{254}K^{255}R^{261}$ of α_3, $T^{335}G^{336}Y^{337}G^{338}I^{340}D^{443}$ are in end-tip between helix $\alpha_{5/6}$, $R^{351}T^{355}E^{359}$ in α_6; $P^{442}E^{443}C^{444}K^{445}$

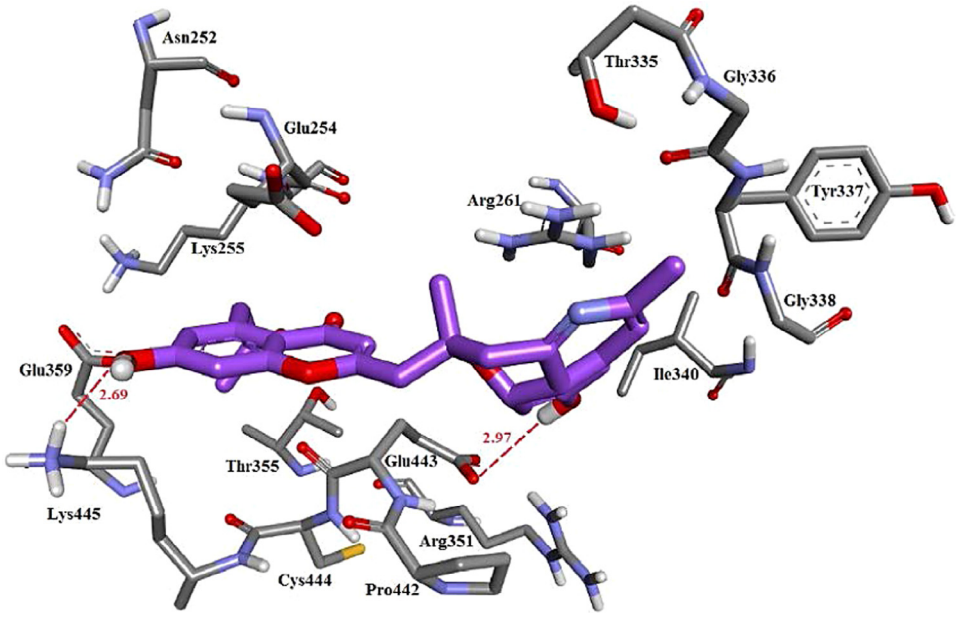

Fig. 20. Interactive binding pose of *R*-Cassiarin-D (purple) with *Pf*MSPDBL2.

Table 6
Physiochemical evaluation of various isoforms along with the quinine alkaloids.

Molecule	a_acc	a_don	a_don_acc	a_aro	*log*$P_{(o/w)}$	*log*S	Mol_wt
Chloroquine	2	1	3	10	4.28	−3.78	319.8
Primaquine	3	2	5	10	2.21	−2.24	259.3
Amodiaquine	3	2	5	16	4.57	−4.49	355.8
Mefloquine	3	2	5	10	4.27	−4.53	378.3
Cassiarin-A	2	1	3	10	2.18	−3.18	213.2
Cassiarin B	2	0	2	0	2.90	−4.04	313.3
Cassiarin B (R_2 = Phenyl)	1	0	1	6	4.22	−5.25	289.3
Cassiarin C	3	1	4	10	2.24	−2.67	215.2
Cassiarin D	6	2	8	16	3.40	−5.75	445.4
Cassiarin E	5	2	7	20	4.15	−6.13	426.4
Cassiarin F	5	3	8	22	4.84	−7.45	427.4
Cassiarin G	5	1	6	10	2.30	−3.13	259.2
Cassiarin H	5	0	5	0	2.59	−3.88	359.3
Cassiarin J	6	2	8	10	2.10	−2.89	333.3
Cassiarin K	2	1	3	10	2.85	−4.01	247.6
DHB	2	0	2	0	2.12	−3.18	216.2

a_acc: number of *H*-bond acceptor atoms; a_don: number of *H*-bond donor atoms; a_don_acc: number of *H*-bond acceptor + donor atoms; a_aro: number of aromatic atoms; *log*$P_{(o/w)}$: Log water/octanol partition coefficient; *log*S: log solubility in water; mol_wt: molecular weight of molecule.

in loop between $\alpha_{8/9}$. Also shows, the *H*-bond donor-acceptor interactions with COOH of Glu443(2.97 Å) and NH_2 terminal of Lys445 (2.69 Å), see in Fig. 20.

In our interest, we evaluated the physicochemical properties of these isoforms with regards to the known quinine alkaloid analogues (Chloroquine, Primaquine, Amodiaquine, Mefloquine). However, most of the Cassiarins show equivalent physicochemical properties with respect to the quinine analogous, while Cassiarin-C found to be the closest candidate with Primaquine, as shown in Table 6.

4. Conclusion

The search for new antimalarial scaffold still have valuable weightage. Current research identified the most putative targets for Cassiarin alkaloids in *P. falciparum*. We also produce a series of top 25 putative targets for individual Cassiarin isoforms against *P. falciparum* (provided in Supplementary information). Also, found that the monomer forms (like Cassiarins C and DHB) have comparatively more cavity fitting to these proteins, as attributed by their smaller surface area than their *Bis*-forms (D, E, and F) (provided in Table 2). However, their multi-mode interactions with their putative protein targets also indicate their synergistic pharmacological mode of action against *P. falciparum* strains. We also disclosed various comparative studies of identified protein targets with their homologous proteins, especially human homologous proteins, which were never studied before and therefore draws several key structural features and differences that could be further exploited in designing and selective targeting against these identified proteins, as provided in case of Oxoacyl acyl-carrier-protein reductase, Kelch motif associated protein, Armadillo repeats only protein and Methionine aminopeptidase 1b. We also found that the screening based on inverse docking, using three different docking methods, quite helpful in filtering the pseudo-positive results which are usually generated from one docking method. This kind of methodology could be useful in, the exploration and target identification for polypharmacological active compounds or validating the side targets of a particular drug.

Conflicts of interest

The authors declare no conflict of interest.

Appendix A. Supplementary material

Supplementary data associated with this article can be found, in the online version, at https://doi.org/10.1016/j.jsps.2018.01.017.

References

Ballut, L., Violot, S., Shivakumaraswamy, S., Thota, L.P., Sathya, M., Kunala, J., et al., 2015. Active site coupling in Plasmodium falciparum GMP synthetase is triggered by domain rotation. Nature Commun. 6, 8930.

Belluti, F., Perozzo, R., Lauciello, L., Colizzi, F., Kostrewa, D., Bisi, A., et al., 2013. Design, synthesis, and biological and crystallographic evaluation of novel inhibitors of *Plasmodium falciparum* Enoyl-ACP-reductase (Pf FabI). J. Med. Chem. 56, 7516–7526.

Bhatt, S., Weiss, D., Cameron, E., Bisanzio, D., Mappin, B., Dalrymple, U., et al., 2015. The effect of malaria control on *Plasmodium falciparum* in Africa between 2000 and 2015. Nature 526, 207–211.

Bhatt, T.K., Khan, S., Dwivedi, V.P., Banday, M.M., Sharma, A., Chandele, A., et al., 2011. Malaria parasite tyrosyl-tRNA synthetase secretion triggers pro-inflammatory responses. Nat. Commun. 2, 1–11.

Bork, P., Sander, C., Valencia, A., 1992. An ATPase domain common to prokaryotic cell cycle proteins, sugar kinases, actin, and HSP70 heat shock proteins. Proc. Natl. Acad. Sci. 89, 7290–7294.

Brown, C., Zhang, K., Emery, J., Prusty, D., Wetzel, J., Heincke, D., et al., 2016. ARO (armadillo repeats only protein) from Plasmodium falciparum. Protein Data Bank.

Bushell, E., Gomes, A.R., Sanderson, T., Anar, B., Girling, G., Herd, C., et al., 2017. Functional profiling of a plasmodium genome reveals an abundance of essential genes. Cell 170, 260–272.

Caniato, R., Puricelli, L., 2003. Review: natural antimalarial agents (1995–2001). Crit. Rev. Plant Sci. 22, 79–105.

Carvalho, D., Paulino, M., Polticelli, F., Arredondo, F., Williams, R.J., Abin-Carriquiry, J.A., 2017. Structural evidence of quercetin multi-target bioactivity: a reverse virtual screening strategy. Eur. J. Pharm. Sci. 106, 393–403.

Chandra, B.R., Olivieri, A., Silvestrini, F., Alano, P., Sharma, A., 2005. Biochemical characterization of the two nucleosome assembly proteins from *Plasmodium falciparum*. Mol. Biochem. Parasitol. 142, 237–247.

Choe, J.-Y., Poland, B.W., Fromm, H.J., Honzatko, R.B., 1999. Mechanistic implications from crystalline complexes of wild-type and mutant adenylosuccinate synthetases from *Escherichia coli*. Biochemistry 38, 6953–6961.

Chofor, R., Sooriyaarachchi, S., Risseeuw, M.D., Bergfors, T., Pouyez, J., Johny, C., et al., 2015. Synthesis and bioactivity of β-substituted fosmidomycin analogues targeting 1-deoxy-D-xylulose-5-phosphate reductoisomerase. J. Med. Chem. 58, 2988–3001.

Choi, H.-J., Loveless, T., Lynch, A.M., Bang, I., Hardin, J., Weis, W.I., 2015. A conserved phosphorylation switch controls the interaction between cadherin and β-catenin in vitro and in vivo. Dev. Cell 33, 82–93.

Cimanga, K., De Bruyne, T., Pieters, L., Vlietinck, A.J., Turger, C.A., 1997. In vitro and in vivo antiplasmodial activity of cryptolepine and related alkaloids from Cryptolepis sanguinolenta. J. Natural Prod. 60, 688–691.

Cleland, W., Kreevoy, M.M., 1994. Low-barrier hydrogen bonds and enzymic catalysis. Science 264, 1887–1890.

Cordeiro, A., Godoi, P., Silva, C., Garratt, R., Oliva, G., Thiemann, O., 2003. Crystal structure of human phosphoglucose isomerase and analysis of the initial catalytic steps. Biochim. Biophys. Acta (BBA) - Proteins Proteomics 1645, 117–122.

Datt, M., Sharma, A., 2014. Conformational landscapes for KMSKS loop in tyrosyl-tRNA synthetases. J. Struct. Funct. Genomics 15, 45–61.

Davis, R.A., Duffy, S., Fletcher, S., Avery, V.M., Quinn, R.J., 2013. Thiaplakortones A-D: antimalarial thiazine alkaloids from the Australian marine sponge Plakortis lita. J. Organ. Chem. 78, 9608–9613.

Deguchi, J., Hirahara, T., Hirasawa, Y., Ekasari, W., Widyawaruyanti, A., Shirota, O., et al., 2012. New tricyclic alkaloids, cassiarins G, H, J, and K from leaves of Cassia siamea. Chem. Pharm. Bull. 60, 219–222.

Deguchi, J., Hirahara, T., Oshimi, S., Hirasawa, Y., Ekasari, W., Shirota, O., et al., 2011. Total synthesis of a novel tetracyclic alkaloid, cassiarin F from the flowers of Cassia siamea. Organic Lett. 13, 4344–4347.

Deguchi, J., Sasaki, T., Hirasawa, Y., Kaneda, T., Kusumawati, I., Shirota, O., et al., 2014. Two novel tetracycles, cassibiphenols A and B from the flowers of Cassia siamea. Tetrahedron Lett. 55, 1362–1365.

Del Carpio, C.A., Takahashi, Y., Sasaki, S.-I., 1993. A new approach to the automatic identification of candidates for ligand receptor sites in proteins:(I) search for pocket regions. J. Mol. Graphics 11, 23–29.

Dowling, D.P., Ilies, M., Olszewski, K.L., Portugal, S., Mota, M.M., Llinás, M., et al., 2010. Crystal structure of arginase from *Plasmodium falciparum* and implications for L-arginine depletion in malarial infection. Biochemistry 49, 5600–5608.

Eaazhisai, K., Jayalakshmi, R., Gayathri, P., Anand, R., Sumathy, K., Balaram, H., et al., 2004. Crystal structure of fully ligated adenylosuccinate synthetase from *Plasmodium falciparum*. J. Mol. Biol. 335, 1251–1264.

Filippova, E.V., Minasov, G., Flores, K., Le, H.V., Silverman, R., McLeod, R.L., et al., 2016. Crystal structure of the ornithine aminotransferase from Toxoplasma gondii ME49 in a complex with (S)-4-amino-5-fluoropentanoic acid. Protein Data Bank.

Frederich, M., Tits, M., Angenot, L., 2008. Potential antimalarial activity of indole alkaloids. Trans. R. Soc. Trop. Med. Hyg. 102, 11–19.

Gileadi, T., Wernimont, A., Hutchinson, A., Weadge, J., Cossar, D., Lew, J., et al., 2011. Crystal structure of Plasmodium falciparum glucose-6-phosphate isomerase (PF14_0341) in complex with fructose-6-phosphate. Protein Data Bank.

Gill, J., Yogavel, M., Kumar, A., Belrhali, H., Jain, S., Rug, M., et al., 2009. Crystal structure of malaria parasite nucleosome assembly protein distinct modes of protein localization and histone recognition. J. Biol. Chem. 284, 10076–10087.

Hodder, A.N., Czabotar, P.E., Uboldi, A.D., Clarke, O.B., Lin, C.S., Healer, J., et al., 2012. Insights into Duffy binding-like domains through the crystal structure and function of the merozoite surface protein MSPDBL2 from *Plasmodium falciparum*. J. Biol. Chem. 287, 32922–32939.

Hu, X., Addlagatta, A., Matthews, B.W., Liu, J.O., 2006. Identification of pyridinylpyrimidines as inhibitors of human methionine aminopeptidases. Angew. Chem. (Int. Ed.) 45, 3772–3775.

Hurley, J.H., 1996. The sugar kinase/heat shock protein 70/actin superfamily: implications of conserved structure for mechanism. Annu. Rev. Biophys. Biomol. Struct. 25, 137–162.

Hurley, J.H., Faber, H.R., Worthylake, D., Meadow, N.D., Roseman, S., Pettigrew, D.W., et al., 1993. Structure of the regulatory complex of *Escherichia coli* III^{glc} with glycerol kinase. Science 259, 673–677.

Iancu, C.V., Borza, T., Fromm, H.J., Honzatko, R.B., 2002. IMP, GTP, and 6-phosphoryl-IMP complexes of recombinant mouse muscle adenylosuccinate synthetase. J. Biol. Chem. 277, 26779–26787.

Jain, A.D., Potteti, H., Richardson, B.G., Kingsley, L., Luciano, J.P., Ryuzoji, A.F., et al., 2015. Probing the structural requirements of non-electrophilic naphthalene-based Nrf2 activators. Eur. J. Med. Chem. 103, 252–268.

Jiang, D.Q., Tempel, W., Loppnau, P., Graslund, S., He, H., Ravichandran, M., et al., 2015. Crystal Structure Analysis of Kelch protein from Plasmodium falciparum. Protein Data Bank.
Jortzik, E., Fritz-Wolf, K., Sturm, N., Hipp, M., Rahlfs, S., Becker, K., 2010. Redox regulation of *Plasmodium falciparum* ornithine δ-aminotransferase. J. Mol. Biol. 402, 445–459.
Kamholz, S.L., 2016. Human emerging and re-emerging infections. Clin. Infect. Dis. 63, 1.
Kayser, O., Kiderlen, A., Croft, S., 2003. Natural products as antiparasitic drugs. Parasitology Res. 90, S55–S62.
Kharkar, P.S., Warrier, S., Gaud, R.S., 2014. Reverse docking: a powerful tool for drug repositioning and drug rescue. Future Med. Chem. 6, 333–342.
Koh, C.Y., Kim, J.E., Napoli, A.J., Verlinde, C.L., Fan, E., Buckner, F.S., et al., 2013. Crystal structures of Plasmodium falciparum cytosolic tryptophanyl-tRNA synthetase and its potential as a target for structure-guided drug design. Mol. Biochem. Parasitol. 189, 26–32.
Kumar, S.P., 2018. PLHINT: A knowledge-driven computational approach based on the intermolecular H bond interactions at the protein-ligand interface from docking solutions. J. Mol. Graph. Model. 79, 194–212.
Kumar, S.P., Jha, P.C., Pandya, H.A., Jasrai, Y.T., 2014. Implementation of pseudoreceptor-based pharmacophore queries in the prediction of probable protein targets: explorations in the protein structural profile of Zea mays. Mol. BioSyst. 10, 1833–1844.
Kumar, S.P., Parmar, V.R., Jasrai, Y.T., Pandya, H.A., 2015. Prediction of protein targets of kinetin using in silico and in vitro methods: a case study on spinach seed germination mechanism. J. Chem. Biol. 8, 95–105.
Kunfermann, A., Lienau, C., Illarionov, B., Held, J., Gräwert, T., Behrendt, C.T., et al., 2013. IspC as target for antiinfective drug discovery: synthesis, enantiomeric separation, and structural biology of fosmidomycin thia isosters. J. Med. Chem. 56, 8151–8162.
Lee, A., Lee, K., Kim, D., 2016. Using reverse docking for target identification and its applications for drug discovery. Expert Opin. Drug Discovery 11, 707–715.
Mac Sweeney, A., Lange, R., Fernandes, R.P., Schulz, H., Dale, G.E., Douangamath, A., et al., 2005. The crystal structure of *E. coli* 1-deoxy-D-xylulose-5-phosphate reductoisomerase in a ternary complex with the antimalarial compound fosmidomycin and NADPH reveals a tight-binding closed enzyme conformation. J. Mol. Biol. 345, 115–127.
Maity, K., Bhargav, S.P., Sankaran, B., Surolia, N., Surolia, A., Suguna, K., 2010. X-ray crystallographic analysis of the complexes of enoyl acyl carrier protein reductase of *Plasmodium falciparum* with triclosan variants to elucidate the importance of different functional groups in enzyme inhibition. IUBMB Life 62, 467–476.
Morita, H., Oshimi, S., Hirasawa, Y., Koyama, K., Honda, T., Ekasari, W., et al., 2007. Cassiarins A and B, novel antiplasmodial alkaloids from Cassia siamea. Organic Lett. 9, 3691–3693.
Morita, H., Tomizawa, Y., Deguchi, J., Ishikawa, T., Arai, H., Zaima, K., et al., 2009. Synthesis and structure–activity relationships of cassiarin A as potential antimalarials with vasorelaxant activity. Bioorg. Med. Chem. 17, 8234–8240.
Müller, I.B., Walter, R.D., Wrenger, C., 2005. Structural metal dependency of the arginase from the human malaria parasite *Plasmodium falciparum*. Biol. Chem. 386, 117–126.
Naidoo, K., 2013. The role of glycerol kinase in Plasmodium falciparum.
Negi, A., 2013. Anaphylactic shock: shocking error of immune system! PharmaTutor 1, 12–16.
Negi, A., Bhushan, S., Gupta, P., Garg, P., Kumar, R., 2013a. Cystathionine β-lyase-like protein with pyridoxal binding domain characterized in leishmania major by comparative sequence analysis and homology modelling. ISRN Computational Biology 2013,
Negi, A., Ramarao, P., Kumar, R., 2013b. Recent advancements in small molecule inhibitors of insulin–like growth factor-1 receptor (IGF-1R) tyrosine kinase as anticancer agents. Mini Rev. Med. Chem. 13, 653–681.
Oliveira, A.B., Dolabela, M.F., Braga, F.C., Jácome, R.L., Varotti, F.P., Póvoa, M.M., 2009. Plant-derived antimalarial agents: new leads and efficient phythomedicines. Part I. Alkaloids. Anais da Academia Brasileira de Ciencias 81, 715–740.
Oshimi, S., Deguchi, J., Hirasawa, Y., Ekasari, W., Widyawaruyanti, A., Wahyuni, T.S., et al., 2009. Cassiarins C– E, antiplasmodial alkaloids from the flowers of Cassia siamea. J. Nat. Prod. 72, 1899–1901.
Oshimi, S., Tomizawa, Y., Hirasawa, Y., Honda, T., Ekasari, W., Widyawaruyanti, A., et al., 2008. Chrobisiamone A, a new bischromone from Cassia siamea and a biomimetic transformation of 5-acetonyl-7-hydroxy-2-methylchromone into cassiarin A. Bioorgan. Med. Chem. Lett. 18, 3761–3763.
Özçelik, B., Kartal, M., Orhan, I., 2011. Cytotoxicity, antiviral and antimicrobial activities of alkaloids, flavonoids, and phenolic acids. Pharmaceutical Biol. 49, 396–402.
Peifer, M., Berg, S., Reynolds, A.B., 1994. A repeating amino acid motif shared by proteins with diverse cellular roles. Cell 76, 789–791.
Pidugu, L.S., Kapoor, M., Surolia, N., Surolia, A., Suguna, K., 2004. Structural basis for the variation in triclosan affinity to enoyl reductases. J. Mol. Biol. 343, 147–155.
Price, A.C., Zhang, Y.-M., Rock, C.O., White, S.W., 2004. Cofactor-induced conformational rearrangements establish a catalytically competent active site and a proton relay conduit in FabG. Structure 12, 417–428.
Saito, T., Ichimura, Y., Taguchi, K., Suzuki, T., Mizushima, T., Takagi, K., et al., 2016. p62/Sqstm1 promotes malignancy of HCV-positive hepatocellular carcinoma through Nrf2-dependent metabolic reprogramming. Nat. Commun. 7, 1–16.
Schnick, C., Polley, S.D., Fivelman, Q.L., Ranford-Cartwright, L.C., Wilkinson, S.R., Brannigan, J.A., et al., 2009. Structure and non-essential function of glycerol kinase in *Plasmodium falciparum* blood stages. Mol. Microbiol. 71, 533–545.
Schumacher, R.-F., Spinelli, E., 2012. Malaria in children. Mediterranean J. Hematol. Infect. Diseases 4, 1–12.
Singla, R., Negi, A., Singh, V., 2014. Indole based alkaloid in cancer: an overview. Pharma. Tutor. Mag. 2, 76–82.
Singla, R., Singh, V., Negi, A., 2013. Synthetic indole alkaloids in cancer: an overview. Adv. J. Pharm. Life sci. Res. 1, 7–15.
Sinnokrot, M.O., Sherrill, C.D., 2004. Substituent effects in π– π interactions: sandwich and T-shaped configurations. J. Am. Chem. Soc. 126, 7690–7697.
Storici, P., Capitani, G., Müller, R., Schirmer, T., Jansonius, J.N., 1999. Crystal structure of human ornithine aminotransferase complexed with the highly specific and potent inhibitor 5-fluoromethylornithine 1. J. Mol. Biol. 285, 297–309.
Thongsaard, W., Chainakul, S., Bennett, G., Marsden, C., 2001. Determination of barakol extracted from Cassia siamea by HPLC with electrochemical detection. J. Pharm. Biomed. Anal. 25, 853–859.
Umeda, T., Tanaka, N., Kusakabe, Y., Nakanishi, M., Kitade, Y., Nakamura, K.T., 2011. Molecular basis of fosmidomycin's action on the human malaria parasite *Plasmodium falciparum*. Scientific Reports 1, 1–8.
VLife, M., 2010. 3.5 (2008) Molecular Design Suite. Vlife Sciences Technologies Pvt. Ltd., Pune
Wells, G.A., Müller, I.B., Wrenger, C., Louw, A.I., 2009. The activity of *Plasmodium falciparum* arginase is mediated by a novel inter-monomer salt-bridge between Glu295–Arg404. FEBS J. 276, 3517–3530.
Wells, T.N., Van Huijsduijnen, R.H., Van Voorhis, W.C., 2015. Malaria medicines: a glass half full? Nat. Rev. Drug Discovery 14, 424–442.
Wernimont, A.K., Artz, J.D., Crombet, L., Lew, J., Weadge, J., Arrowsmith, C.H., et al., 2011. Crystal structure of methionine aminopeptidase 1b from Plasmodium Falciparum, PF10_0150. Protein Data Bank.
Wernimont, A.K., Dong, A., Hills, T., Amani, M., Perieteanu, A., Lin, Y.H., Loppnau, P., Arrowsmith, C.H., Edwards, A.M., Bountra, C., Weigelt, J., Hui, R., 2011. Crystal Structure of PF10_0123, a GMP Synthetase from Plasmodium falciparum.
Wickramarachchi, T., Cabrera, A.L., Sinha, D., Dhawan, S., Chandran, T., Devi, Y.S., et al., 2009. A novel Plasmodium falciparum erythrocyte binding protein associated with the merozoite surface, PfDBLMSP. Int. J. Parasitol. 39, 763–773.
Wickramasinghe, S.R., Inglis, K.A., Urch, J.E., Müller, S., Van Aalten, D.M., Fairlamb, A. H., 2006. Kinetic, inhibition and structural studies on 3-oxoacyl-ACP reductase from *Plasmodium falciparum*, a key enzyme in fatty acid biosynthesis. Biochem. J. 393, 447–457.
World_Health_Organization, 2015. WHO/UNICEF report: Malaria MDG target achieved amid sharp drop in cases and mortality, but 3 billion people remain at risk. Saudi Med. J. 36, 1377–1378.
World_Health_Organization, 2016. World malaria report 2015, World Health Organization.
Wu, H.-Y., Hu, W.-Y., Liu, Q., Yu, Z.-H., Zhan, J.-B., Yan, K.-L., et al., 2016. Three new alkaloids from the twigs of Cassia siamea and their bioactivities. Phytochem. Lett. 15, 121–124.
Yajima, S., Hara, K., Iino, D., Sasaki, Y., Kuzuyama, T., Ohsawa, K., et al., 2007. Structure of 1-deoxy-D-xylulose 5-phosphate reductoisomerase in a quaternary complex with a magnesium ion, NADPH and the antimalarial drug fosmidomycin. Acta Crystallogr., Sect. F: Struct. Biol. Cryst. Commun. 63, 466–470.